MERCURY (II) REMOVAL USING TITANIUM DIOXIDE PHOTOCATALYST

A Thesis

by

MARY ANNA KATEBAH

Submitted to the Office of Graduate and Professional Studies of
Texas A&M University
in partial fulfillment of the requirements for the degree of

MASTER OF SCIENCE

Chair of Committee,	Ahmed Abdel-Wahab
Committee Members,	Bill Batchelor
	Mahmoud El-Halwagi
Head of Department,	Nazmul Karim

August 2015

Major Subject: Chemical Engineering

ABSTRACT

Mercury (Hg) is one of the most detrimental by-products of industrial activities such as fossil fuel combustion and mining. In this study, adsorption and photocatalytic reduction of mercury (II) into elemental mercury using two types of titanium dioxide (TiO_2) was investigated.

Photocatalysis involves a material's ability of creating an electron-hole pair after its exposure to solar radiation with photon energy higher than that of the applied photocatalyst, resulting in free-radicals at the positive holes and electrons at the conduction band. These radicals can efficiently reduce or oxidize certain contaminants. Photocatalysis is a convenient method for reducing mercury (II) since it utilizes inexpensive chemicals and solar energy, an energy source found abundantly in Qatar.

Two different types of titanium dioxide were evaluated for Hg(II) removal: commercially available nanoparticles and synthesized nanotubes. The surface properties of the two types of TiO_2 were characterized using transmission electron microscopy (TEM), scanning electron microscopy (SEM), X-ray photoelectron spectroscopy (XPS), and X-ray diffraction (XRD). To achieve efficient hole-transfer, formic acid was selected as the hole-scavenger in some of the experiments.

Control experiments were performed in the dark to assess the efficiency of photocatalysis versus direct adsorption. Effects of pH, concentration of hole-scavenger, photocatalyst dose, and irradiation time on Hg(II) removal were evaluated.

Experimental results indicate that more Hg(II) removal occurred at higher pH levels and larger photocatalyst doses. Additionally, the use of formic acid enhanced Hg(II) reduction, indicating that it was an efficient hole scavenger for this application. It was also observed that higher efficiencies were obtained using synthesized nanotubes as compared to commercial nanoparticles.

In the dark, results showed near-to-no adsorption of Hg(II) on the nanoparticles, while a small amount of adsorption occurred in the presence of formic acid. On the other hand, significant amount of Hg(II) was adsorbed on the nanotubes due to their high surface area and increased negative surface charge. Higher removals in the light as compared to dark conditions are clear evidence that photocatalysis is taking place and that TiO_2 is an efficient photocatalyst for treating water contaminated with Hg(II).

DEDICATION

To my parents, who taught me the joys of learning and the value of education. Their sacrifices made me the person I am today.

To my husband, Joel, for his never-ending love and support.

ACKNOWLEDGEMENTS

I would like to express my deep gratitude to Dr. Abdel-Wahab, my advisor, for his time and guidance. He has been there for me since my freshman year at the university; from teaching me my first chemical engineering class and offering me my first student-research job, to mentoring me during my master's education. I am very thankful for all he has done for me. I am also grateful for my committee members, Dr. Bill Batchelor and Dr. Mahmoud El-Halwagi for their help and insight.

I would also like to thank Dr. Dong Suk Han for being an excellent lab mentor. His optimism and passion for teaching and helping others have inspired me to become a better researcher. I am grateful for our undergraduate research assistant, Ali Mansour, for his commitment and hard work. I would also like to thank Yuhang Duan, Dr. Theis Solling and Dr. Yiming Wubulikasimu for their assistance in the surface characterization analyses. I am also thankful for all my friends and colleagues at Texas A&M University for making this journey an enjoyable one.

I am grateful for my siblings, for making life full of joy and laughter. Special thanks to my parents for shaping me into the person I am today; my father for being the best role-model a person can have, and my mother for always being there for me. Her faith, love and guidance have pushed me to be the best in everything I do. I am also very grateful for my husband, Joel, for his patience and support. His love, as a husband, friend and father, has given me a whole new meaning to life. I would also like to thank my baby daughter, Alexandra, for adding life to my life!

NOMENCLATURE

C_{in}	Initial Metal Concentration (mg/L)
C_f	Final Metal Concentration (mg/L)
CVAAS	Cold Vapor Atomic Adsorption Spectrometry
DI Water	Deionized Water
E_{CB}	Conduction Band Potential
E^o	Standard Reduction Potential
FA	Formic Acid
Hg	Mercury
h_{vb}^+	Valence Band Holes
K_d	Distribution, or Partition, Coefficient
LM	Liquid Membrane
MDL	Method Detection Limit
MEUF	Micellar Enhanced Ultrafiltration
MHBB	Modified *Hardwickia Binata* Bark
NaOH	Sodium Hydroxide
PEUF	Polymer Enhanced Ultrafiltration
pI	Isoelectric Point
Ppb	Part per Billion
Ppm	Part per Million
RO	Reverse Osmosis

RPM	Revolutions per Minute
SLM	Supported Liquid Membrane
r_{ws}	Ratio of Water to Solid (mL/g)
SEM	Scanning Electron Microscopy
TDS	Total Dissolved Solids
TEM	Transmission Electron Microscopy
Ti-NT	Titanium Dioxide Nanotubes
UF	Ultra-filtration
XPS	X-Ray Photoelectron Spectroscopy
XRD	X-Ray Diffraction

TABLE OF CONTENTS

Page

Page

LIST OF FIGURES

Page

Page

LIST OF TABLES

Page

1. INTRODUCTION

Water sustainability is a major global challenge for the 21st century. Approximately 1.2 billion people, almost one-fifth of the world's population, are facing physical water scarcity. Another quarter of the world's population is facing economic water shortage [1]. Scarce water resources in the Middle-East region have caused an increasing growth of water demand [2]. Qatar, in particular has limited freshwater resources and thus water security has been greatly emphasized in the Qatar National Research Strategy (QNRS) of the Qatar National Vision (QNV) 2030 [3]. Maximizing water reuse/recycle and minimizing wastewater discharges in the country can alleviate the stress of its limited freshwater supplies and the environmental impact caused by wastewater discharges.

One of the challenges of achieving water security is ensuring that the water is treated to meet specific quality standards. To accomplish this, undesired contaminants have to be removed from the water. Mercury, a toxic and bio-accumulative chemical, is one of the most detrimental pollutants found in industrial wastewater, making it a major concern worldwide. Highly reactive mercury (II) (Hg(II)) salts are the most toxic form of mercury [4]. Hg(II) salts can be converted by sulfate-reducing bacteria, Fe (III)-reducing bacteria or methanogens, into methylmercury [5], a neurotoxic substance that poses a health risk to humans through the aquatic food chain [4]. A major source of mercury contamination occurs as a result of disposing industrial mercury-containing wastes into the aquatic system, causing it to settle in the bottom sediments of the

receiving water bodies [6]. Therefore, it is of utmost importance to remove Hg(II) from industrial waste before discharging it into the waterways [4].

Conventional methods of removing Hg(II) from aqueous solutions include activated carbon adsorption, ion exchange, precipitation, reverse osmosis and biological treatment, amongst others. Although these methods have been able to remove Hg(II), disadvantages of these technologies include either large chemical requirements or high energy demands. Recently, semiconductor photocatalytic processes activated by solar energy have become a promising alternative for removing contaminants from water and wastewater [6]. Development of these solar-driven technologies will assist in the reduction of water treatment costs and carbon footprint.

Titanium dioxide (TiO_2) is one of the most common photocatalysts due to its chemical stability, nontoxicity, and low cost. Its photocatalytic properties are associated with the formation of photogenerated charge carriers (electrons and holes) that occur as a result of the absorption of light with photon energy greater than the band gap energy of the TiO_2 ($\approx$ 3.12 eV, an equivalence to a wavelength of 388 nm). Photogenerated holes in the valence band diffuse to the surface and react with the water molecules to form hydroxyl radicals by water oxidation. While the holes and the hydroxyl radicals participate in oxidizing nearby organic molecules on the photocatalyst surface, electrons in the conduction band reduce electron-deficient compounds in the solution [7]. Figure 1 illustrates a general photocatalytic redox process.

In this research, photocatalytic reduction of mercury (II) to elemental mercury powered by solar energy was investigated using TiO_2 photocatalyst. Additionally, a

comparative study using TiO_2 nanoparticles and synthesized nanotubes was performed. Effects of irradiation time, solution pH, and photocatalyst type and dosage on Hg(II) removal were also evaluated.

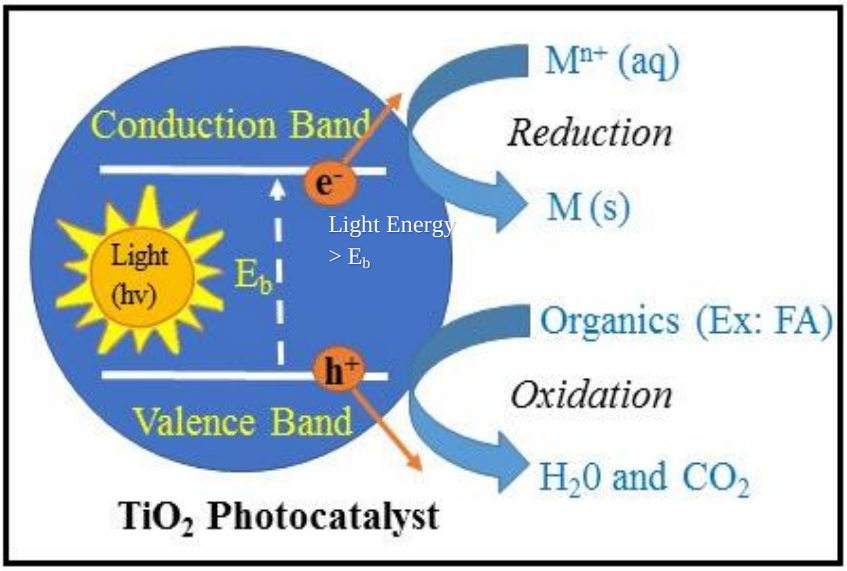

Figure 1: General photocatalysis redox process

2. LITERATURE REVIEW

2.1 Mercury

2.1.1 Background

Mercury is released into the environment via natural occurring and anthropogenic activities. Natural sources of mercury such as volcanoes, forest fires, thermal springs and natural deposits, contribute to about one third of current mercury air emissions [8]. However, human activities have released significant amounts of mercury via coal combustion in power plants, landfills, industrial and manufacturing activities. Other sources of mercury that can lead to its release to the environment include its usage in barometers, thermometers, dental products (amalgam), electrical devices and fungicides. Moreover, mercuruous chloride ($HgCl_2$), one of the oldest known pharmaceuticals, is continuously used as an antiseptic. Thimerosal ($C_9H_9HgNaO_2S$), another antiseptic containing 49.5% ethyl mercury, has been used for years as a preservative in infant and flu vaccines [8]. Published data indicate that human activities have almost tripled the amount of mercury in the atmosphere in the past hundred years. [9]

Mercury exists in three oxidation states: elemental (Hg(0)), monovalent (Hg^{+}) and divalent mercury (Hg^{2+}). In the atmosphere, gaseous mercury is present in its elemental form. Elemental mercury is generally less soluble and can travel across long distances before being oxidized and released back to the environment. However, mercury is found primarily in its divalent form in aqueous solution [9].

In solution, aqueous mercury speciation depends on several factors such as pH, redox potentials, and chloride concentration. In the case of divalent mercury, the major species found in highly acidic solutions is $HgCl_2$. As the solution pH increases up to 4.5, a small amount of HgClOH starts to form. The most significant aqueous specification change occurs at pH 7, where $HgCl_2$ and $Hg(OH)_2$ as well as HgClOH become the existing species, with $Hg(OH)_2$ being the predominant one until it becomes the only major species at pH levels above 8.5 (Figure 2) [10].

Human exposure to all different forms of mercury occurs through various pathways, with each form affecting human health in a different way. While the highest exposure to humans results from elemental mercury, it is the least toxic form on a kilogram-for-kilogram basis. Therefore, research is now more commonly targeted towards removing mainly the aqueous forms of mercury [11].

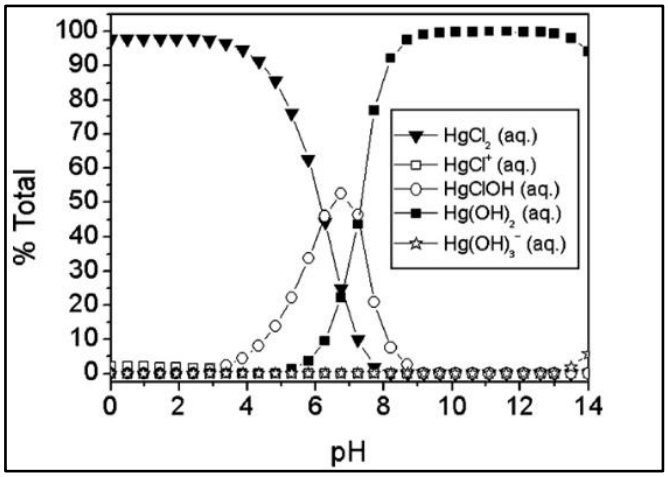

Figure 2: Chemical Speciation of Mercury [10]

Figure 3 depicts a simplified mercury cycle, where mercury in the form of elemental vapor (Hg^0) is released into the atmosphere via natural or human-instigated activities. Air circulation in the atmosphere widely disperses it, where it could be photo-oxidized to the inorganic divalent mercury form (Hg^{2+}) by atmospheric oxygen [9]. These ions can further combine with water vapor and migrate through rainfall back into the earth, where they settle in the soil and water. Processes such as forest fires can release it from the soil back into the atmosphere. Otherwise, it can combine with sulfides and deposit as cinnabar (HgS). In aquatic bodies, inorganic mercury is ingested by anaerobic microorganisms thus converting it into methylmercury where it can be taken up by other aquatic organisms. Methylmercury (CH_3Hg) concentration is enhanced through higher trophic levels, ultimately resulting in significant exposure to humans [9].

While mercury exposure can occur via inhalation or dermal contact, the primary form of exposure to humans is by fish consumption. The presence of mercury as a cation, such as methylmercury, allows it to react with most ligands in living cells, causing severe damage. Elemental mercury is the least toxic form of mercury. Its stability allows it to pass through the digestive system without reacting with living cells [12]. On the other hand, methylmercury can react with cysteine to form a compound that is similar in nature to methionine, a crucial amino acid that enters the brain barrier to synthesize proteins in the body. Consequentially, when methylmercury enters the body, it can penetrate the brain inhibiting protein formation [12].

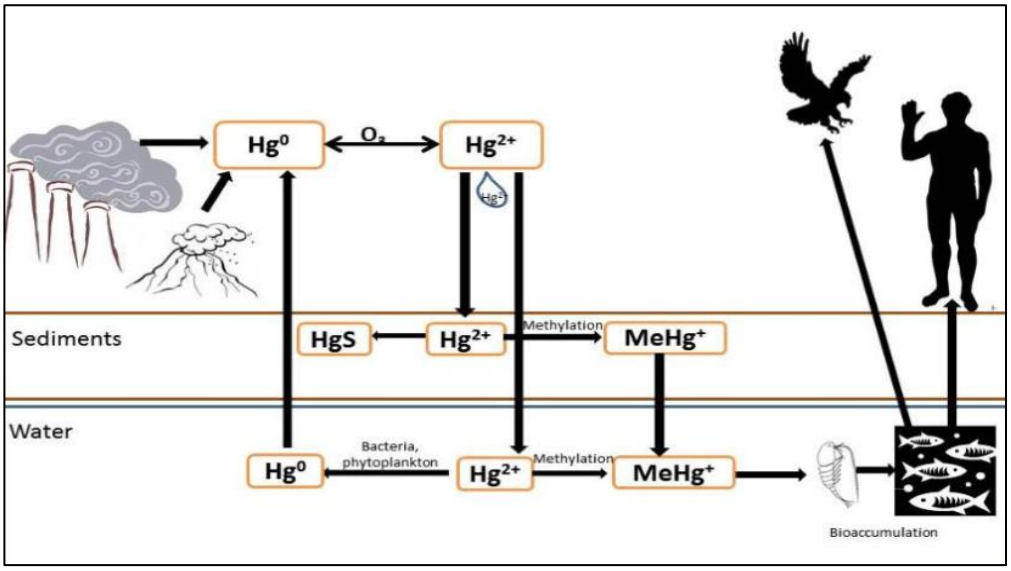

Figure 3: Mercury Cycle in the Environment [9]

Methylmercury can also cause permanent damage to the brain, kidneys, and fetuses in pregnant women. Major symptoms of mercury poisoning include headaches, nausea, vomiting, numbness, impaired vision and hearing amongst others. Young children and fetuses are most vulnerable to its effects and can experience a series of development issues including palsy, retardation, seizures and death. Mercury toxicity was not understood until the mid-1900s when the population of Minamata in Japan developed neurological problems as a result of contamination by wastewater that was discharged from a fertilizer company. Impacts of the disaster were extremely severe that deaths continued for years after the event [12]. This makes mercury removal a priority in the area of environmental engineering.

2.1.2 Mercury Control Regulations

Several statutes have been developed to regulate mercury emissions in the United States, including the Clean Air Act (CAA), Clean Water Act (CWA), Resource Conservation and Recovery Act (RCRA) and Safe Drinking Water Act (SDWA) [13].

As a result of the CAA amendments that were passed in 1990, industries that release mercury are required to install technologies that limit the mercury release to maximum achievable control technology standards (MACT) [14]. Thirty years later, the EPA announced new regulations for coal-fired power plants to protect public health [15]. The United States Environmental Protection Agency (USEPA) set the maximum contaminant level (MCL) for mercury to be 2 µg/L in drinking water. [16].

Stringent regulations have also been enforced in other countries. For instance, Norway banned the use of mercury in the manufacturing and importation/ exportation of mercury products in 2008 [17]. The same year, Denmark prohibited the use of dental mercury amalgam except for molar surface fillings in permanent teeth [18]. One year later, Sweden banned all products containing mercury [19]. Around the same time, the European Union banned mercury from being used in non-electronic measuring instruments including thermometers and barometers [20].

Internationally, the United Nations Environment Program (UNEP) initiated a Minamata Convention on Mercury, where 140 countries agreed to prevent mercury emissions [21].

Regulatory limits for Hg(II) in wastewater discharges depend on the region and the industry. For instance, Flanders set a maximum discharge limit between 0-150 ppb,

depending on the industry, and a quality standard of 1 ppb for surface water and ground water [22]. One of the strictest limits for mercury discharge is for refinery wastewater in the State of California, USA, where a monthly average of 0.079 ppb must not be exceeded. The most stringent limit for any water discharge is 0.0013 ppb, set for the Great Lakes of the United States and Canada [23]. In Qatar, the treated wastewater limits range from 1-2 ppb depending on the final discharge point [24]. Consequently, the removal of mercury from water in general, and wastewater in specific, is vital.

2.1.3 Current Technologies for Mercury Removal

Conventional techniques that are currently being used for the removal of aqueous mercury include precipitation [25], coagulation/ co-precipitation [26], ion-exchange [27], adsorption [16], chemical reduction [28], membrane separation [25]. Examples of emerging technologies are biological treatment systems [29], membrane extraction processes [25], and photocatalysis [4, 10, 30]. The use of a specific technology depends on several factors including the initial mercury concentration, type of generated waste, and overall efficiency/cost effectiveness. A brief summary describing each of the aforementioned techniques will be presented in the following sub-sections.

2.1.3.1 Precipitation

Precipitation and coagulation/co-precipitation technologies are some of the most commonly used techniques for mercury removal from wastewater. The most common method for precipitation involves the addition of sulfide salts to waste streams in order to convert soluble mercury into relatively insoluble mercury sulfide according to the

following reaction (Equation 1) [25]. Table 1 summarizes published results for Hg(II) removal by sulfide precipitation.

$$Hg^{2+} + S^{2-} \rightleftharpoons HgS\ (s)\ (1)$$

Table 1: Published data for the removal of Hg(II) salts by sulfide precipitation [25]

	Mercury Concentration (µg/L)				
Treatment Chemical	**Initial**	**Final**	**Percent Mercury Removal**	**Treatment pH**	**Additional Treatment**
Sodium sulfide	N/A	<3	NA	NA	Vacuum filter
	300-6,000	10-125	58-99.8	NA	Pressure filter
	1,000-50,000	10	99.9	N/A	Flocculation + activated carbon
Sodium hydrosulfide	13,150	20	>99.9	3.0	Filter
Magnesium sulfide	5,00-10,000	10-125	99-99.9	10-11	None
Sulfide Salt	300-6,000	10-125 (50 avg)	58-99.8	5.1-8.2	Filtration
	NA	100-300	NA	NA	None
	NA	100	NA	NA	None
	NA	42297	NA	NA	Activated carbon

This process is often combined with additional processes such as pH adjustment and flocculation, followed by solid separation. Separation techniques include gravity settling and filtration. Figure 4 illustrates a conventional process flow diagram for Hg(II) precipitation using sulfide [25].

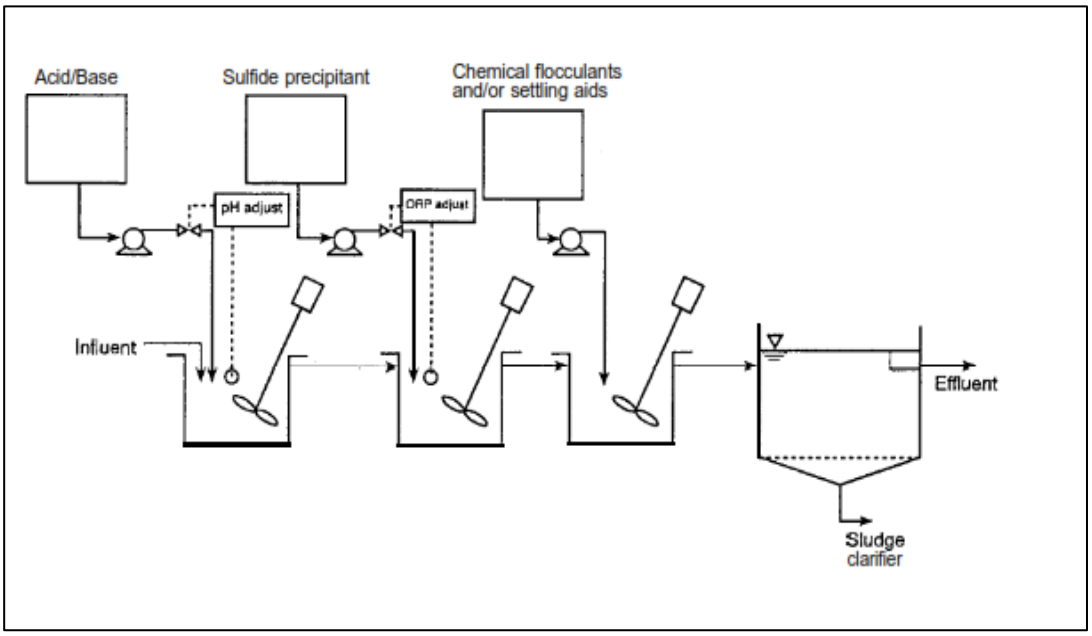

Figure 4: Process flow diagram for Hg(II) precipitation using sulfide [25]

Sulfide precipitation can achieve greater than 99% Hg(II) removal for initial mercury levels that are higher than 10 mg/L. Even when this process is combined with post-treatment technologies, the final Hg(II) concentration ranges between 10-100 µg/L, values that are still above the regulatory limits. Other restrictions to this process include the solution pH; the performance of sulfide precipitation peaks at neutral pH levels and drops down at pH levels greater than 9. Nevertheless, sulfide precipitation remains the

most common technique for aqueous mercury removal in numerous chlor-alkali plants with reported percent removals between 95-99.9% [25].

Other disadvantages to this process include the following [25]:

i. Formation of soluble mercury sulfides at high sulfide concentrations
ii. Difficulty in monitoring instantaneous reactor sulfide levels
iii. Formation of toxic sulfide residuals in the treated water streams
iv. Difficulty in clarifying, processing and disposing the generated sludge
v. Mercury resolubilization from sulfide sludges at the landfill storage conditions (Potential ground-water pollution issue)

2.1.3.2 Coagulation/ Co-Precipitation

Several coagulants are used to remove aqueous mercury from water including aluminum sulfate (alum, $Al_2(SO_4)_3$), iron salts and lime. When alum or iron is used as a coagulant, the best mercury removal mechanism is most likely via adsorptive co-precipitation. In this technique, mercury can be adsorbed on aluminum hydroxide or iron hydroxide solids formed by the addition of alum or iron salts, respectively. This process is isothermal and the efficiency can be improved by the formation of optimal bulk solids and by pH adjustments to enhance the surface charge of the bulk solid and the aqueous-phase mercury speciation [25].

Published data for the treatment of inorganic mercury in domestic sewage streams showed that iron and alum co-precipitation, followed by filtration, reduced the

initial mercury levels of 50-60 µg/L by 94-98% [26]. When lime, followed by filtration, was used as a coagulant to treat water with initial mercury (II) concentration of 500 µg/L, 70% mercury removal was achieved. Separate use of alum and iron for the treatment of water streams with 50 µg/L of initial Hg(II) concentrations achieved 47% and 93-98% removal percentages, respectively [26]. This shows that co-precipitation has a synergistic effect on Hg(II) removal from water. Table 2 summarizes published data for coagulation/ co-precipitation treatment processes [25].

Table 2: Coagulation/co-precipitation data for Mercury (II) removal [25]

		Mercury Concentration (µg/L)				
Coagulant Salt	**Coagulant Dosage (mg/L)**	**Initial**	**Final**	**% Mercury Removal**	**Treatment pH**	**Additional Treatment**
Alum	1,000	11,300	102	99	3	Filtration
	100	90	11	88	NA	-
	100	NA	10	NA	NA	-
	21-24	5.9-8	5.3-7.4	10-34	6.7-7.2	Filtration
	NA	50	26.5	47	7	Filtration
	220	60	3.6	94	6.4	Filtration
	20-30	3-8	1.5-6.4	50-81	NA	-
	20-30	3-16	2.3-21.3	<23	NA	-
	34-72	4-5	2.5	38-50	6.9-7.4	Filtration
Iron	NA	50	3.5	93	8	Filtration
	40	50	1	98	6.2	Filtration
	20-30	1-17	0.5-6.8	50-97	NA	-
	20-30	2-17	1.2-12.8	40-93	NA	-
Lime	415	500	150	70	11.5	Filtration
	NA	0.66	0.2	>69	8.3	-

NA = Not Available

2.1.3.3 Ion Exchange

Cationic mercury can be selectively exchanged over calcium and magnesium using resins that contain the iminodiacetic group. However, this process is unselective towards copper and cobalt. Anionic complex forms of mercury, such as $HgCl_3^-$, can be removed using anion exchange resins. Duolite GT-73, a thiol resin, is selective for mercury in all of its oxidation states [25].

Most of the ion exchange technologies consist of packed columns that carry out four main operations in a complete ion exchange cycle: service, backwash, regeneration and washing. The first step involves contacting the ion exchange resin in the column with a mercury-contaminated water stream. The ion exchange resin is said to be spent as soon as the maximum allowable effluent mercury concentration is reached. This is followed by a backwash step to expand the bed and dispose of the fines that may be causing bed clogging. To regenerate the spent resin, a reverse exchange process occurs by contacting it with a concentrated solution of the original exchange ion. Finally, the last step disposes of any excess regeneration solution before the column is operated again for the next cycle [25].

Advantages of the ion exchange process include the following [25]:

i. Ability to operate on demand
ii. High insensitivity to process variability
iii. Availability of a large variety of specific resins
iv. Beneficial selectivity reversal after resin regeneration

On the other hand, this process is associated with several disadvantages including [25]:

i. High potential for chromatographic effluent peaking
ii. Formation of spent regeneration brine that requires disposal
iii. Inconsistency in the effluent quality
iv. Inability to function with water containing high TDS levels

Historically, the ion exchange technology was limited to anion resins for the treatment of wastewater containing inorganic mercury in the mercuric-chloride form. The process is effective in the presence of high chloride content waters such as those generated in chlor-alkali plants. This results in the formation of negatively charged mercury chloride complexes. If the chloride content of the water is low, the process efficiency can be enhanced by the addition of chlorine or chloride salts [25].

Cation exchange of mercury can be efficient if the wastewater contains a low anion content. Amberlite IR-120 and Dowex-50W-X8 are two of the most effective cation exchange resins used for mercury removal from industrial wastewater. Duolite GT-73, a cationic resin, can also react with ionic mercury. The thiol functional group found in this resin has a very high selectivity for mercury and a strong tendency to remove other metal ions such as copper, silver, lead and cadmium [25].

Chelate resins, primarily insoluble polymers attached to a complexing group(s), with high mercury removal capacities have been reported. These can bond metal cations within its structure to form a metal-containing chelate. This reaction consists of both ion exchange and chemical reactions. Examples of chelate resins include Duolite ES-466,

Nisso Alm-525, Purolite S-920, and Diaion CR-10. Some of these resins, such as Purolite S-920, can follow pre-filtration to remove mercury from ground water with concentrations as low as 1 µg/L [25]. However, this process maintains the disadvantage that it produces variable effluent qualities and is limited to waters with low TDS levels. Furthermore, some types of resins are readily oxidizable, thereby reducing their longevity [31].

2.1.3.4 Adsorption Processes

High mercury removal efficiencies can be achieved by adsorption processes [16]. Due to its high efficiency and good mechanical resistance, activated carbon is one of the most commonly used adsorbents for mercury removal [32]. Recently, however, the use of other adsorbents including processed vegetable or mineral materials (ex. Bicarbonate-treated hull carbon), Modified *Hardwickia Binata* Bark (MHBB), magnetic chitosan, coal fly ash, Forager sponge, and metal hydroxides have been reported. However, when metal hydroxides are used as adsorbents, the process is more commonly referred to as coagulation or co-precipitation as described in section 2.1.4.2 [16].

One of the advantages of adsorption is the increase in removal efficiencies as a result of incremental adsorbent dosage. Due to the adsorbent's isothermal or quasi-isothermal behavior, diminishing residual soluble concentrations are shown as the dosage of the adsorbent increases. However, this results in the generation of wastewater treatment residuals that require disposal, unless adsorbent recovery is facilitated. Other variables that can affect the efficiency of these processes are the adsorbent type, wastewater pH and contaminant speciation [16].

2.1.3.5 Chemical Reduction

The standard electrode potential of each metal determines where it is placed in the electromotive series, a list of elements in decreasing order of standard potentials. The higher the value of the standard reduction potential, the easier it is for the metal to be reduced. For instance, aqueous mercury can be removed from solution by reducing it using a metal that is higher in the electromotive series. The solid produced in this step can be removed by a separation process such as filtration. Examples of chemical reducing agents that can be used for mercury removal are aluminum, zinc, iron, hydrazine, stannous chloride, and sodium borohydride [25].

Although research results have been published regarding reduction processes, their industrial applications are still limited. While the primary advantage of chemical reduction processes is mercury recovery in its elemental form, their main disadvantage is their inability of efficiently removing mercury to concentrations less than 100 µg/L [25].

Gould et al. conducted bench-scale experiments to treat mercury-containing-water using iron wire. Although their results showed high removals (96-99%), residual concentrations in the treated effluent were still undesirable (22-33 mg/L) due to the high initial concentration (735-2,030 mg/L) [33]. On the other hand, experiments performed by Garu and Bisang on wastewater (100 mg/L initial concentration) with iron felt produced by iron wool compression achieved treated effluents with 68-91 µg/L residual mercury levels [28].

Recent work by Looney et al. showed that this process can be applied to water with low mercury concentrations (138 ng/L) using stannous chloride or tin(II) chloride.

However, low reagent doses with Sn:Hg ratio of 1:1 showed little to no removal. High dosages (Sn:Hg ratios 5-25:1), showed almost complete removal yielding final concentrations of 10 ng/L mercury. Limitations to this process include the requirement of relatively high amounts of chemicals and the presence of trace levels of tin in the effluent water [34].

2.1.3.6 Membrane Separation

Examples of membrane processes that have been applied for aqueous mercury removal include ultrafiltration, charged filtration, crossflow microfiltration (CFMF), magnetic filtration, and reverse osmosis. Ultrafiltration (UF), a pressure-driven membrane process that utilizes porous membranes for removing dissolved and colloidal matter, differs from reverse osmosis (RO) mainly by the magnitude of pressure applied to operate the process, with the former operating at a relatively lower operating pressure than the latter. UF is typically used for the removal of colloidal material and large molecules with molecular weights greater than 5,000. Treated effluents from UF using spiral wound elements can be further purified using an additional RO step [25].

Enhancements to the conventional ultrafiltration process have also been studied such as the polymer enhanced ultrafiltration (PEUF) technology [35] and the micellar enhanced ultrafiltration (MEUF) [36]. PEUF is based on the complexation of heavy metals with water-soluble polymers such as polyethylenimine and its derivatives, including polyvinylamine, polyacrylic acid, polyvinyl alcohol, polyvinyl acetate and polyvinyl pyrolidone. Since the UF pores are smaller than the added polymeric agents,

generated complexes can be separated from the water, allowing the treated effluent to pass through the membrane.

Since this process only uses one aqueous phase, problems that arise with multiphase separation processes (such as mass-transfer limitations, interface reactions and membrane instability) are avoided. An advantage of this process is the relatively low-energy requirement [35], enhanced removal efficiency, high binding selectivity and the formation of a highly concentrated metal retentate that can be re-used. On the other hand, disadvantages to this process include finding appropriate polymers for complexation, studying the removal in the presence of other metal ions in the water and optimizing the ratio of metal to polymers. While there are numerous publications associated with this process, its application in the industry is yet to be developed [36].

Similarly, MEUF is aiming to enhance the performance of the regular UF technology. A surfactant is added into a contaminated solution until its concentration reaches beyond its critical micellar concentration (CMC), causing the formation of large micelles that capture the relatively small-sized contaminants. Consequently, the contaminated micelles get retained by the UF membrane [37]. To increase contaminant retention, surfactants have to be chosen with electric charge opposite to that of the contaminant. For instance, sodium dodecyl sulfate, an anionic surfactant, is often used for the removal of heavy metals such as mercury[38]. Alka et al. observed that the rejection of mercury using MEUF increased by increasing pressure. A maximum rejection of 94% occurred at an optimum pressure, flow rate and feed concentration conditions of 4 atm, 16 l/min and 5 ppm, respectively. This showed that MEUF was

effective in separating mercury from water [38]. However, one of the primary drawbacks of MEUF and PEUF technologies is the leakage of low molecular weight surfactant monomers or poly-electrolytes through the membrane [39].

Charged membrane ultrafiltration can be also employed for mercury removal. This method uses a noncellulosic, high flux, negatively charged membrane. The charge is a result of dissociated subgroups in the membrane structure. An advantage to this method is the reduction of membrane fouling due to the negative polarization [25].

CFMF, also known as Exxflow, is a solid-liquid separation process that uses a dynamic membrane as a filtration medium. Pressure differences across the membrane allow the liquid phase to pass through, while retaining the solids until they are flushed by the residual flow [25]. The microfilter is made up of a series of tubes that are 2.5 cm in diameter. The treated effluent is pumped at turbulent velocities down the center of the tubes, where a downstream valve generates enough backpressure to force the clarified water through the microporous membrane [23].

A representation of the cross-flow microfilter is illustrated in Figure 5 [25]. Usually, the concentrate, or the dewatered suspended solids, are recycled to the feed tank to enhance the concentration of the suspended solids. Part of this concentrate stream is continuously removed from the system, typically to a clarifier, for further solid de-watering [23]. Reported efficiencies for Hg(II) removal using CFMF range from 41.3 to 99.8% with initial mercury concentrations of 150-1,270 µg/L [40].

A downside to UF and CFMF is the requirement of process feed pretreatment as these technologies cannot remove mercury from the solution merely by size exclusion [25].

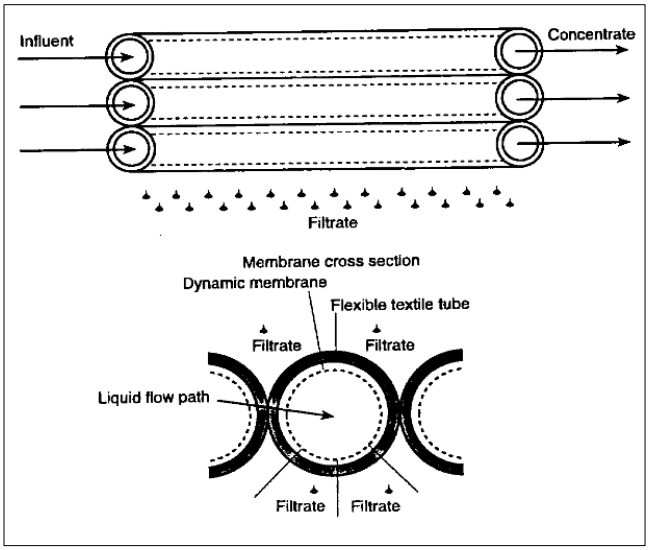

Figure 5: Illustration of the Cross-Flow Microfilter **[25]**

In magnetic filtration, mercury is removed by the formation of a magnetic precipitate by coagulating and adding magnetic seed. The wastewater is then passed through a filter composed of ferromagnetic wires that generate a magnetic field. An advantage to this process is the removal of fine precipitates as the process does not depend on pore size exclusion. The strong magnetic forces act on the magnetic particles with sufficient force as they move through the magnetic field despite the competing gravitational, hydrodynamics and inertia forces. Reported values for mercury removal from a waste stream containing 15 mg/L Hg(II) range between 99.2-99.8% [41]. Advantages of these systems include their high efficiency rates, economical

attractiveness and environmental-friendliness. However, their main disadvantage is that they only filter magnetic particles [42].

Reverse osmosis (RO) depends on applying pressure higher than the inherent osmotic pressure of the solution to force water to permeate through a semi-permeable membrane, thereby rejecting most of the dissolved solids. The pressures applied in reverses osmosis range from 200 to 800 psi. The process is substantially affected by fouling, scaling, pH-temperature-pressure-related hydrolysis and membrane deterioration. Feed water requirements to the RO system are very stringent, particularly with respect to the suspended solids concentration that can foul the membrane surfaces. Published results for the removal of 5 and 9 mg/L inorganic mercury showed 82.4 and 83.3% removal respectively [25]. However, Mullett et al. reported effluent mercury concentrations of < 10 ug/L after treating a waste stream with 30 mg/L, achieving more than 99% removal [43].

Liquid membrane (LM) technologies are more recent membrane separation processes that have been used to remove inorganic mercury from water. LM consists of a homogenous, non-porous, thin film composed of organic liquid trapped between two aqueous phases of different compositions. The solute transfers from one phase through the other across the LM as a result of concentration differences across the membrane. There are two main types of LM: supported (SLM) and non-supported liquid membranes [44].

SLM consists of a hydrophobic porous membrane support placed between two aqueous phases. Certain components can pass from one phase to another through the

LM/SLM via diffusion. Considerable research efforts have been conducted to study the LM based processes to separate mercury from solution. Combinations of diluent-carriers were used such as chloroform-microcyclic ligands, dichloromethane-calixarene nitril, n-parrafins-oleic acid, and a range of 80-100% mercury removal was observed. Most of the processes employed were non-supported LM. However, an advantage of SLM compared to the non-supported LM is its ease in construction and operation [44].

Another type of LM technology is the microemulsion liquid membrane process, where a microemulsion is formed by the addition of oleic acid tetradecane, DNP-8 surfactant and 6N sulfuric acid to water contaminated by mercury. Membrane separation of the microemulsion produces an aqueous and an emulsion phase. Demulsifying the aqueous phase produces another waste stream that that is high in mercury concentrations [31].

While the membrane processes discussed above are able to remove inorganic mercury from water, they are associated with several disadvantages including the following [31]:

i. The processes generally consist of several steps or stages
ii. High pressures and costs are required
iii. Secondary waste streams are produced as by-products
iv. Membrane fouling adds complexity to the processes

2.1.3.7 Electrochemical Technologies

Electroremediation treatment has been a successful method for mercury (II) removal from soil and groundwater. It works by applying an electric field or direct

current through an anode and a cathode that are inserted in wells, usually containing an electrolyte, to enhance conductive properties of the electric field [45]. The electric signal allows the mineralization of organic compounds, such as volatile organics and metal contaminants, by polarizing the soil causing the soil particles to charge and discharge electricity. As a result, redox reactions are initiated at the interfaces within the system (containing soil, groundwater, contaminant and electrodes) that enhance metal mobilization and organics mineralization. Metals move towards the electrodes where they are deposited and removed from the soil/groundwater system [46].

Although electroremediation technologies are often named interchangeable with electrokinetic treatments (EKT), there are a number of differences between them. First, lower energy levels are necessary to perform remediation as compared to EKT technologies. Second, electroremediation treatment is only effective within months instead of years. Additionally, metals usually move towards and deposit on both electrodes as opposed to EKT where metals transfer to only one electrode [46].

Advantages to these technologies include the following [46]:

i. Viable in-situ technology for the treatment of inorganic and organic compounds in porous media
ii. Adsorption of ionic contaminants to sediment particles that are difficult to remove by simple water flushing
iii. High efficiencies and cost-effectiveness

However, these processes are associated with several limitations, including [46]:

i. Limitation by the solubility of the contaminants. For instance, heavy metals in their metallic forms are difficult to separate from the soil samples
ii. Inefficiency when the contaminant concentration is low compared to the non-target ion concentration
iii. Problems arising from acidic pH levels and anode corrosion in-situ
iv. Proportional dependence on the grain size; higher performance is exhibited in clays and silts than in sands and gravels
v. Limitation of the drilling technology affiliated with electrodes installation

2.1.3.8 Biological Treatment

Microorganisms have been used to remove metals from contaminated wastewater, mining water, and industrial wastes. For instance, mercury can be reduced to its elemental form by a mercury-resistant *Pseudomonas Putida* strain of bacteria. This step can be followed by volatilization to remove the elemental mercury from solution [47]. Mercury can also be precipitated using sulfate-reducing bacteria. Other forms of mercury removal using biological techniques involve mercury adsorption; for instance, *Pseudomonas Aeruginosa* and *Bacillus Thuringiensis* possess charged microbial cell surfaces and mercury can be extracellularly accumulated on their cell

walls. Additionally, inactivated, nonliving microbes possess biosorbent properties that allow them to adsorb mercury [48].

While these processes are capable of removing mercury, they exhibit downsides such as slow reaction rates, requirement of biomass acclimation, creation of optimal growth conditions and nutrients provision to the microbes. After treatment, the effluent is usually treated with activated carbon to remove residual mercury. Moreover, the process generates waste residuals, primarily dead bacteria and elemental mercury, which require disposal [16].

2.1.3.9 Other Processes for Mercury Removal

Additional methods for mercury removal from water include chemical leaching, stabilization and amalgamation, and nanotechnology [49].

Chemical leaching involves the addition of leaching solutions, such as nitric acid, hypocholorous acid and sulfuric acid, to water containing mercury. These acids are chosen due to their ability to readily dissolve elemental and inorganic mercury. When the leaching solution gets in contact with the water, solubilized ionic mercury is formed. The leachant is then removed, collected and treated to convert the mercury into its elemental form [49].

Stabilization technologies were used to treat mercury wastes with less than 260 mg/kg of total mercury [49]. When the concentration of mercury is greater than that, separation processes were used to recover the mercury. There are various immobilization processes that are used for mercury treatment and they generally fall under two main categories: stabilization and amalgamation. Stabilization processes either immobilize

mercury through chemical bonds to form a fixed matrix, or convert it to an immobile species, thereby decreasing vaporization or leaching to the surrounding environment. An advantage of this technology is the formation of a more stable mercury compound. However, one of its drawbacks is its inability of reducing the total mercury concentration. Instead, it reduces mercury leachability, forming a product that requires disposal [49].

Amalgamation, on the other hand, is a physical technology that is only applicable to elemental mercury, where another metal forms a semisolid alloy with mercury by dissolving into the metal, forming a solid solution [49].

Recently, nanoscale technologies have shown promising results in removing mercury from water. While their application is still limited to the laboratory and pilot-scales, their use at the field scale is predicted to eventually grow as research develops and the cost of nanotechnology decreases [31].

2.2 Nanotechnology for Aqueous Mercury Removal

Nanotechnology is an effective solution to solve water-related issues in terms of both quality and quantity. Nanomaterials are currently being utilized in advanced water treatment processes, providing more efficient and economically-feasible technologies for treating water/wastewater to meet the stringent water quality standards [50].

Nanomaterials possess innovative and modified physical, chemical and biological properties as a result of their structural characteristics, enhanced reactivity and adsorption capacities, and higher surface area-to-volume ratios. These properties allow them to treat water/wastewater more efficiently than the conventional methods.

Examples of applications of nanotechnology in water/wastewater treatment includes: adsorption, disinfection, membranes and photocatalysis. Detailed explanations are provided in Table 3. Currently, several nano-based technologies are being studied to remove heavy metals and other contaminants, such as mercury, from water.

Various nanomaterials are being used to remove mercury from water such as iron oxide (hematite, magnetite and maghemite) [51, 52], alumina [53], chitosan coated magnetic nanoparticles, gold supported on alumina nanoparticles [54], Manganese dioxide nanowhiskers [55], carbon nanotubes, metal (Ti, Zn) oxides, cadmium and zinc sulfides [56], polymeric nanoadsorbents and others [52]. However, one of the most commonly used material mercury removal is titanium dioxide photocatalyst. It offers several advantages compared to the other materials listed previously such as its high photocatalytic activity in the solar spectrum, its low toxicity, high stability and selectivity and low cost [50].

Table 3: Applications of nanotechnology in water and wastewater treatment [50]

Applications	Examples of nanomaterials	Some of novel properties
Adsorption	CNTs/ nanoscale metal oxide and nanofibers	High specific surface area, selective and more adsorption sites, short intraparticle diffusion distance, tunable surface chemistry, easy reuse, and so forth.
Disinfection	Nanosilver/ titanium dioxide (Ag/ TiO_2) and CNTs	Strong antimicrobial activity, low toxicity and cost, high chemical stability ease of use, and so forth.
Photocatalysis	Nano-TiO_2 and Fullerene derivatives	Photocatalytic activity in solar spectrum, low human toxicity, high stability and selectivity, low cost, and so forth.
Membranes	Nano-Ag/TiO_2/Zeolites/Magnetite and CNTs	Strong antimicrobial activity, hydrophilicity low toxicity to humans, high mechanical and chemical stability, high permeability and selectivity, photocatalytic activity, and so forth.

2.3 Photocatalysis

2.3.1 General Principle of Photocatalysis

Photocatalysis is used in various research areas, particularly the energy and environmental fields. The photocatalytic properties of materials have been used to change solar energy into chemical energy for the oxidation or reduction of certain materials to produce useful products such as hydrogen and hydrocarbons, and for the removal of contaminants and bacteria from air and water [7].

By definition, photocatalysis is the acceleration of a photoreaction by a catalyst [57]. Photocatalytic reactions exist in two main categories: homogenous and heterogeneous reactions. In homogenous photocatalysis, the reactants and the photocatalysts are present in a uniform phase. Examples of these systems include Fenton

and Fenton-like processes. On the other hand, the reactants and the photocatalysts exist in different phases in heterogeneous photocatalysis. This includes numerous reactions such as oxidation, dehydrogenation, hydrogen transfer, $^{18}O_2$–$^{16}O_2$ and deuterium-alkane isotopic exchange, metal deposition, water detoxification, and gaseous pollutant removal. Hg(II) photoreduction using TiO_2 is an application of heterogeneous photocatalysis for water detoxification [58].

In heterogeneous photocatalysis, reactions occur at the surface of the photocatalyst. Heterogeneous processes can be further divided into two categories, catalyzed and sensitized photoreaction processes, depending on where the initial excitation takes place. In catalyzed photoreactions, the initial photoexcitation occurs in an adsorbate molecule which then reacts with the ground-state catalyst substrate, whereas in sensitized photoreactions, the initial photoexcitation takes place on the catalyst substrate that transfers an electron and/or energy, into a ground state molecule. The initial photoexcitation step is followed by the transfer of either electrons, or energy, or both. It is the second step (energy or electron transfer) that leads to chemical reactions in the heterogeneous photocatalytic processes [58].

Various chemicals have been used as photocatalysts, such as chalcogenides (metal sulfides) or metal oxides among which are titanium dioxide (TiO_2), zinc oxide (ZnO), cadmium sulfide (CdS), pyrite (FeS_2), and zinc sulfide (ZnS). Published results indicate that the best photocatalytic performances are mostly achieved using titania [59].

Photocatalysis offers many advantages compared to the conventional methods that require relatively large chemical or energy requirements and are associated with the

formation of large quantities of waste by-products. Photocatalytic reactions require source of light energy such as solar energy; one of the most abundant form of energy found in the world. Additionally, reactions can be carried out in mild temperature and pressure conditions, an advantage that is of special importance when the substrates or products are heat sensitive or explosive. Another advantage of requiring low temperatures is the isolation and identification of reactive intermediates, thereby providing insight into the mechanisms of the reaction pathways in complex reactions [60].

Drawbacks to photocatalysis include fast recombination reactions that limit the efficiency of these processes, and catalyst rupture that can lead to termination of the reactions [60]. However, research has found methods to overcome these issues, such as adding hole scavengers to the systems [61], doping the photocatalysts with certain materials (such as that silver) to prevent electron hole recombination [62] and changing the shape of the photocatalyst [63].

Recently, efforts have been made to study the feasibility of recycling the catalyst to minimize chemicals and costs associated with this process. Costa et.al. used hydrothermally synthesized TiO_2 nanotube photocatalysts for the degradation of indigo carmine dye. After their photodegradation reactions, the photocatalysts were filtered, washed with water and added to a photoreactor to be re-used in another solution of indigo carmine dye. Results revealed that the nanotubes maintained 90% of their activity after 10 reaction cycles, giving this photocatalyst an advantage of easy recovery [64].

Due to the efficiency of photocatalytic processes and their cost-effectiveness, the applications of photocatalytic processes in information recording, solar energy conversion, environmental contaminant degradation, and organic compound synthesis are expected to enhance drastically over the years [60].

2.3.2 Titanium Dioxide photocatalysis

Titanium dioxide is one of the most commonly used and investigated photocatalysts due to its strong oxidizing properties, high ability to decompose organic pollutants, superhydrophilicity, chemical and thermal stability, enhanced durability, low toxicity and cost-effectiveness and transparency to light. Examples of applications for TiO_2 photocatalysis are summarized in Figure 6 [7].

Titanium dioxide can be used to reduce Hg(II) into a less harmful state that is deposited or adsorbed by the photocatalyst and subsequently extracted (by chemical or mechanical means) into a form that can be further treated or safely disposed [65].

Titanium dioxide naturally exists in three main polymorphic forms: anatase, brookite and rutile, with the anatase form having the highest overall photocatalytic activity [66]. Although extensive research was undertaken to explain the differences between the photocatalytic activity of the different TiO_2 polymorphs, reasons for anatase exhibiting higher photocatalytic activity compared to the rest are still being debated [67]. Possible explanations include the following:

i. Anatase TiO_2 has a larger band-gap than the rutile form. This causes an increase in the oxidation ‘power’ of the electrons, thus facilitating electron transfer from TiO_2 to the adsorbed

material [68].

ii. Anatase TiO_2 is associated with an indirect band gap that is smaller than the direct one. The fundamental band gap of rutile TiO_2 is direct. In the cases where rutile TiO_2 does exhibit an indirect band gap, it would be very similar to the direct one. Semiconductors that have indirect band-gaps have longer charge carrier life times relative to the materials that have direct gaps. Since anatase has a longer electron-hole pair life, it would present higher photocatalytic activity [68].

It was reported that a synergistic effect between anatase and rutile titanium dioxide exists, where the addition of rutile can substantially enhance the photocatalytic activity of the anatase form for contaminant degradation [69]. Commercially, an example of titanium dioxide that possesses both forms is P25. Initially fabricated by Degussa Co, P25 TiO_2 contains an anatase-to-rutile ratio of approximately 3:1 [70].

The photocatalytic properties of TiO_2 are a result of the formation of photogenerated electrons and holes, or charge carriers, that form after the adsorption of solar light with photon energy greater than the band gap energy of TiO_2. The valence band holes diffuse to the photocatalyst's surface and react with the adsorbed water molecules to form hydroxyl radicals (·OH). The generated radicals and holes oxidize organic molecules on the TiO_2 surface. At the same time, electrons in the conduction bands react with molecular oxygen to form superoxide radical anions ($O_2^{\cdot -}$) that undergo subsequent reduction reactions [7].

TiO_2 surfaces are superhydrophillic, with reported contact angle values less than 5^o when UV-irradiated [7]. As described above, most of the valence band holes react directly with the adsorbed species (mostly electron-rich compounds) or water forming hydroxyl radicals. However, some of the holes are trapped at lattice oxygen sites and can react with titanium dioxide itself, weakening the bonds between the lattice titanium and oxygen ions. These bonds can also be interrupted by water molecules to form new hydroxyl groups that are less stable and possess higher surface energy, thereby resulting in the superhydrophilicity of TiO_2 surfaces [7].

Considerable attention has been directed towards the construction of TiO_2 structures in the nano- and micro-scale. Examples of fabricated TiO_2 nanomaterials that have been used in photocatalysis, dye-sensitized solar cells, lithium- ion batteries and electrochromic displays include spheres, nanorods, fibers, tubes, sheets, and interconnected architectures. The photocatalytic performance of these nanomaterials depends on numerous factors such as the size, specific surface area, pore volume and structure, crystalline phase, and exposed surface. Therefore, research has been largely focused on developing enhanced photocatalytic nanomaterials by optimizing the aforementioned characteristics [7].

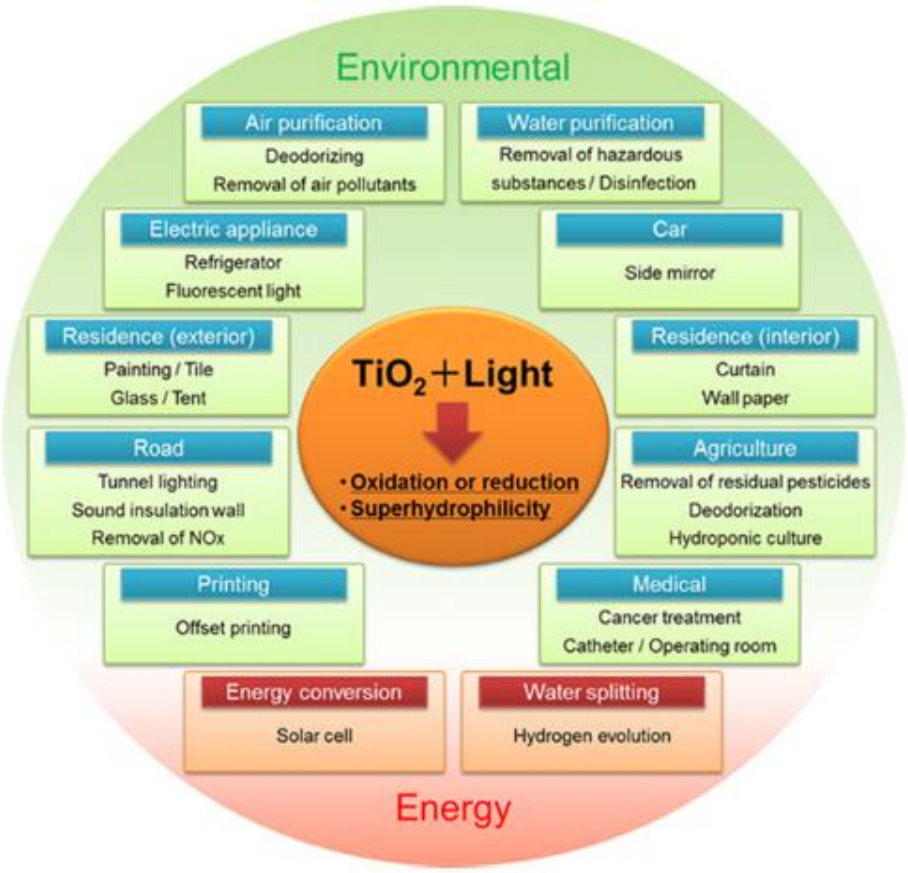

Figure 6: Applications of TiO_2 photocatalytic processes [7]

2.3.3 Synthesis of titanium dioxide nanotubes

Conventionally, titanium dioxide is used in the form of nanoparticles with a relatively high surface area. However, the photocatalytic performance of these nanoparticles is limited by the fact that TiO_2 has its maximum light absorption in the UV range, in addition to its high charge-carrier recombination rate [65]. These drawbacks can be overcome by modifying the structure of the TiO_2 nanoparticles into nanotubes. In addition to having even higher surface area and an increased tendency for light absorption, their tubular structure decreases the number of boundaries among the TiO_2 nanotubes compared to the nanoparticles, causing enhanced charge carrier transportation [71]. Additionally, nanotubes have shown promising results towards catalyst re-use and recycling. When TiO_2 nanoparticles and nanotubes were tested for their recyclability, the nanotubes maintained 90% of their activity after 10 cycles, whereas the nanoparticles lost their activity on the second cycle. Thus, the nanotubes present greener chemistry than the nanoparticles [64].

As a result, more efforts have been focused towards the development of efficient routes to manufacturing titania nanotubes with controllable dimensions.

Several methods have been followed to synthesize nanotubes with various geometrical shapes and microstructures, such as the sol-gel method, anodization, electrodeposition, sonochemical deposition, and hydrothermal treatment. For instance, a sol-gel processing technique produced nanotubes with diameters ranging from 70 to 100 nm [72], while anodic oxidation produced nanotubes with an inner diameter of 100 nm

and length of 200 nm. Kasuga et al. reported that nanotubes with a diameter and length of 8 and 100 nm respectively were produced by chemical treatment [73].

Recently, alkali hydrothermal treatment has shown promising application for the production of nanotubes, where the main mechanism of nanotube synthesis depends on the wrapping of intermediate multi-layered titanate nanosheets driven by the mechanical stress produced during the crystallization or dissolution. The advantage of this method is the ease in controlling parameters such as temperature, pressure, process time, chemical concentration, pH and others. Furthermore, the simplicity of this one-pot process and its reproducibility makes it a more appealing choice for nanotube manufacturing. This technique is named as a soft-chemical technique since the reactions occur at relatively low temperatures [74].

The conventional hydrothermal treatment method usually requires high pressures and temperatures, long reaction times, and complex preparation procedures. Recently, microwave irradiation has been found to be a more efficient and improved method compared to the conventional hydrothermal treatment for the preparation of inorganic materials. The microwave-assisted treatment method offers the advantage of more uniform, rapid and volumetric heating. Additionally, the microwave-assisted hydrothermal method significantly reduces the reaction time and temperature, leading to rapid crystallization and method simplification [75].

Wu et al. investigated the effect of various experimental variables on the fabrication of titanium dioxide nanotubes, including reaction time, sodium hydroxide concentration, and raw material precursors. Their results showed that, at constant

microwave power of 195W, TiO_2 nanotubes were synthesized with short heat treatment and low temperature when anatase or rutile TiO_2 precursor was treated with 8-12N NaOH for more than one hour. TEM results showed hollow, open-ended and multi-layered wall structures with 8-12 nm diameters and 200-1000 nm lengths [72]. Similar research was conducted by Moloto et al. where P25 TiO_2 powder was treated with 18M sodium hydroxide in a microwave oven, at a pressure of 22 bars, for 15 minutes. Results showed the presence of a mixed crystalline phase with anatase, rutile, and Ti_4O_7 present. The structure was tubular with average diameters of 25 nm [76].

In summary, the micro-wave assisted hydrothermal method is an efficient and cost-effective method for the production of TiO_2 nanotubes from nanoparticles [72].

2.3.4 Photocatalytic reduction of mercury using titanium dioxide photocatalyst

Mercury reduction by heterogeneous photocatalysis using oxide semiconductors, such as ZnO, TiO_2, WO_3 under UV, visible and solar irradiation has been widely studied. Published results showed that the reduction efficiency of mercury depends on several factors such as substrate adsorption, intermediates reactivity, illumination intensity, irradiation time, catalyst dosage, initial contaminant concentration, solution pH levels, presence of oxygen, addition of organic donors, and others [61].

Studies by Litter et al. compared titanium dioxide photocatalysis for the treatment of three different types of mercuric salts such as $Hg(NO_3)_2$, $HgCl_2$, and $Hg(ClO_4)_2$. The products formed on the photocatalyst's surface were either Hg(0), HgO or calomel, depending on the experimental conditions. Kinetic studies of Hg(II) reduction over irradiation time showed that initial conversion was very rapid, and was

followed by a decrease or rate arrest. Different pH levels were studied (pH 3, 7 and 11) and their results showed that faster reduction occurred at higher pH levels for all types of salts [61].

The net stoichiometric reaction for metallic mercury deposition was reported to be [61]:

$$Hg(II) + H_2O \rightarrow 2H^+ + \frac{1}{2}O_2 + Hg(0) \text{ (2)}$$

A direct reductive pathway for mercury reduction involving successive one-electron charge transfer reactions was postulated:

$$Hg(II) + e^- \rightarrow Hg(I) \text{ (3)}$$

$$Hg(I) + e^- \rightarrow Hg(0) \text{ (4)}$$

However, the reduced mercury species can be reoxidized by photogenerated positive holes or hydroxyl radicals as shown below [61]:

$$Hg(0/I) + hole^+ / HO\bullet \rightarrow Hg(I/II) \text{ (5)}$$

This fast recombination rate of the photogenerated electrons and positive holes presents a limitation to the photocatalytic reduction of mercury. Methods that are used to mitigate the recombination rate include deposition of metal oxide or doping of novel materials on the titanium dioxide surface, and the addition of a hole or electron scavenger to the reaction. Both methods are used to deviate the photogenerated electrons and holes away from the surface of the metal oxide. This enhances the charge carriers' lifetimes, giving them enough time to start the reduction and oxidation reactions respectively [77].

In most photocatalytic reduction processes, the addition of a hole scavenger to the system is vital. Several chemicals have been used as hole scavengers, or sacrificial donors. EDTA was found to be a very effective reductant since it forms stable complexes with Hg(II). Other hole scavengers that were investigated include: citrate, ethanol, sodium dodecyl sulfate (SDS), cetyltrimethylammonium bromide, formic acid and other organic acids [61].

One of the advantages of using formic acid over the others is its small size, making it easier to adsorb onto the titanium dioxide photocatalyst for direct oxidation. Additionally, the photoproducts of formic acid oxidation are water and carbon dioxide, products that do not generally lead to major environmental issues [30].

3. METHODOLOGY

3.1 Development of experimental and analytical methods

The development of experimental and analytical procedures was a fundamental step that assisted in achieving the primary research objective. This included the following subtasks:

1. Experimental set-up: Preparation of a batch reactor system exposed to artificial solar irradiation
2. Preparation of samples, mercury stock and standard solutions
3. Synthesis and characterization of titanium dioxide nanotubes (Ti-NT)
4. Development of an analytical procedure to measure mercury using cold vapor atomic adsorption spectrometry (CVAAS)

Table 4 summarizes the tasks and the methodologies that are required to meet the research objectives.

Table 4: Research plan summary

Task	Methodology	Expected Benefits
Task 1: Development of the experimental and analytical methods	• Prepare a batch reactor system exposed to artificial solar irradiation • Synthesize and characterize Ti-NT • Develop procedure for measuring Hg(II) using CVAAS	Ensure reliable experimental procedures and reproducible analytical methods
Task 2: Characterization of the kinetics of Hg(II) reduction	• Conduct batch kinetic experiments with varying operating parameters including: type and dose of TiO_2, solution pH, and the addition of hole scavengers	Find the optimum operating conditions for the photocatalytic reduction of Hg(II)

3.1.1 Experimental Set-up

A reactor (1-L glass beaker) containing mercury and TiO_2 was set up under a solar simulator (Figure 7). Throughout the entire experimentation phase, sunlight was simulated (AM 1.5G; 1 Sun) using a 150-W Xenon Arc Lamp. Experiments were performed aerobically in a fume hood. P25 TiO_2 nanoparticles have been supplied by Sigma Aldrich and are approximately 25 nm in diameter with a surface area of about 50 m^2/g. The expected relatively high photocatalytic activity of the nanoparticles is related to its high surface area since it is known that photocatalytic activity is enhanced with increasing surface area [78]. To further enhance surface area, the nanoparticles were modified into nanotubes as detailed in the subsequent sections.

The reaction volume was maintained at 500 ml in all the experiments. The solid suspension was stirred at approximately 200 RPM for the duration of the tests. Samples were withdrawn at regular time intervals and filtered through two 0.45 micron (47 mm diameter) mixed cellulose ester filter papers purchased from Advantec.

Adsorption experiments were conducted in the dark under similar conditions set for the irradiated experiment as control tests for mercury removal. For these experiments, the glass beakers were entirely wrapped with aluminum foil and placed on the stir plate at the same RPM as the illuminated experiments. The purpose of these experiments was to evaluate mercury adsorption by TiO_2 versus mercury photoreduction.

Photocatalyst and hole scavenger dosage was varied throughout the experimentation according to the experimental plan. Additionally, experiments were designed to study the performance of the modified titanium dioxide nanotubes as compared to that of the conventional commercial titanium dioxide.

Solution pH was adjusted using dilute hydrochloric acid (3M HCl) for acidic conditions and sodium hydroxide (1M NaOH) for alkaline conditions.

After sample collection, the vials were wrapped in aluminum foil and stored in the dark, and mercury analysis was performed within twenty-four hours after collection.

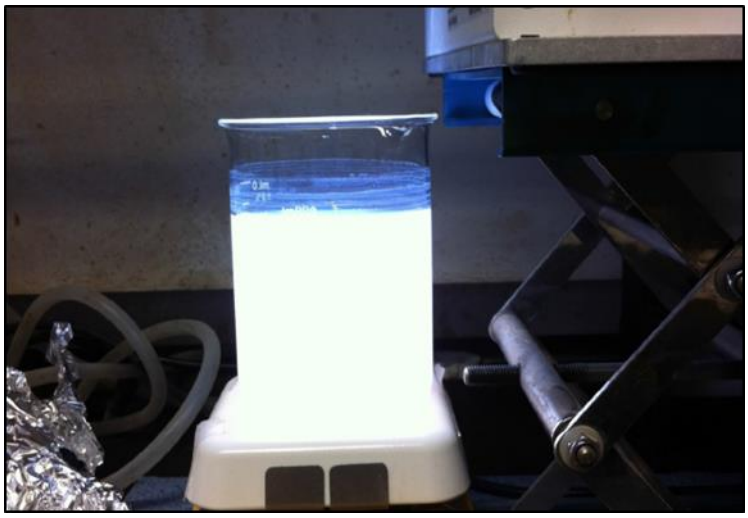

Figure 7: Experimental Set-up

3.1.2 Preparation of samples, mercury stock and standard solutions

Mercury (II) stock solutions (1,000 mg/L) were prepared from mercury (II) chloride (supplied from Sigma Aldrich) in deionized water (DI water). The stock solution was used for the experiments and preparation of standards. To prevent the mercury in the stock from adsorbing to the walls of the container, the solution was acidified using HCl to pH less than 2.

Fresh standard solutions were prepared prior to each atomic adsorption analysis; 1 mg/L of mercury was prepared as a stock solution for the standards. A calibration curve was made using 5, 10, 30 and 60 µg/L mercury solutions that were prepared by a stepwise dilution method. One- ml and five- ml micropipettes were used for the preparation. A preliminary precision and accuracy test was performed to determine the

effectiveness of CVAAS for measuring mercury. Results for this test are shown in Section 4.1.

3.1.3 Synthesis and Characterization of Titanium Dioxide Nanotubes

The performance of TiO_2 nanoparticles for Hg(II) reduction was compared to that of the synthesized Ti-NT. The nanotubes were synthesized and characterized prior to performing experimentation to verify their photocatalytic properties. Nanotubes were produced by a hydrothermal process using a highly alkaline sodium hydroxide (NaOH) solution [79].

First, 400 g/L (10N) NaOH was prepared and allowed to cool down to room temperature. Next, 5g of TiO_2 powder were added and the mixture was stirred until a homogenous suspension was observed. The suspension was treated for one hour at 1,600 W power in a MARS microwave digestion system (MARSXpress™ vessel) obtained from CEM. After treatment, a vacuum filtration assembly was used to separate the nanotubes from the alkaline solution. During filtration, the sample was washed with distilled water until the pH of the filtrate reached neutral levels, ensuring that the NaOH was washed out of the Ti-NT surface.

Initially, the filtered nanotubes were dried overnight at 30ºC in a dry oven. After drying, the nanotubes agglomerated together forming a cake-like structure. This caked layer was grinded using a mortar and pestle to be used for the experiments. However, this process caused the properties of the nanotubes to be compromised and decreased the surface area of the nanotubes due to the agglomeration. Results supported this observation, as described in Section 4.3.2.2. Alternatively, a stock suspension of

nanotubes in DI water was prepared to be used for Hg(II) reduction experimentation. This suspension did not require drying prior to its utilization.

The concentration of TiO_2 in the suspension was determined by weight difference. Five 3-ml samples were collected in glass vials and dried overnight at 30ºC until they were completely dry. The weight of the vials was measured before sample addition and after sample drying. The average weight of the five samples was calculated to be 0.0614 g. (Table 5). The average TiO_2 concentration (20.5 g/L) in the suspension was found by dividing the average weight by the volume (3 ml).

Prior to each experiment, the stock suspension was magnetically stirred for thirty minutes to ensure homogeneity and consistency before using it for Hg(II) reduction experiments.

The surface properties of the two types of TiO_2 were characterized using surface analysis techniques, including X-ray diffraction (XRD), transmission electron microscopy (TEM), scanning electron microscopy (SEM) and X-ray photoelectron spectroscopy (XPS).

Table 5: Mass of TiO_2 measured after drying five 3-ml samples of the stock suspension

Sample Number	Mass of TiO_2 remaining after drying 3ml of stock suspension (g)
1	0.0616
2	0.0611
3	0.0619
4	0.0608
5	0.0616
Average	**0.0614**

3.1.4 Analytical Method for Mercury Measurement

Mercury was analyzed primarily using CVAAS technique, in which the mercury (II) was reduced to its elemental form before the analysis. This is the most widely used method for mercury quantification and it offers several advantages over other methods including its simplicity, low-cost of operation and high sensitivity and selectivity.

As the objective of this study is to maximize the removal of mercury from water, the total mercury content was measured. Therefore, sodium borohydride was used as a reductant to reduce all forms of mercury to its elemental form. A continuously flowing carrier stream (5N HCl solution) carried the sample to the manifold from the injection loop in an acid hydride system, where it mixed with the reductant (10% $NaOH/NaBH_4$). The mixture was then combined with an argon stream and carried to the gas/liquid

separator. The gas phase passed first through the wash flask to remove soluble contaminants and then through a drying tube to remove liquid droplets. The carrier gas then transported the Hg(0) vapor to the spectrometer where its absorbance was measured at a wavelength of 253.7 nm [80].

Prior to each analysis, mercury concentrations in known standards were measured using CVAAS. Mercury absorbance was plotted against concentration (in μg/L) to create a calibration curve that was used as the basis for the mercury concentration quantification in the samples. If the Pearson Coefficient of Determination (r^2 value) of the curve was less than 0.99, the graph was discarded and a new curve using fresh standards was prepared.

Due to the CVAAS method's sensitivity towards too high or too low mercury concentrations, samples were diluted with DI water to ensure that the final mercury concentration was approximately towards the center of the calibration curve. To eliminate any residual Hg within the lines of the spectrometer, each sample was followed by DI washing until no mercury absorbance was observed.

3.2 Characterization of the kinetics of Hg(II) reduction

Chemical behavior and rate of Hg(II) removal from water was characterized as affected by irradiation time, photocatalyst type (nanoparticles, nanotubes) and dosage (0.01, 0.05, 0.1, 1.0 g/L), and pH levels (pH 4, 8, 10). The effect of each of these variables was investigated while keeping others constant. Samples were taken at different reaction times and analyzed for mercury as described in the previous sections.

The hole scavenger that was used in this study was chosen to be formic acid. Based on the results from the tests described above, experiments under best conditions were performed with the addition of formic acid with the following concentrations: 0.25 and 2.5 mM. Control experiments with the addition of formic acid were performed in the dark to quantify the removal of mercury via photocatalysis as compared to complexation with formic acid.

3.3 Chemicals and reagents

Table 6 lists the chemicals that were used in this study and their specifications. All solutions were prepared with DI water (18Ω) generated from EMD Millipore's Milli-Q Integral Water Purification System.

As for the laboratory glassware and equipment clean-up, the following procedure was followed: first, they were soaked for 24 hours in a warm cleaning solution of 2% laboratory detergent, then they were soaked for 24 hours in 1% HCl, and finally they were thoroughly washed and rinsed with DI water followed by air-drying overnight.

Table 6: Chemicals used and specifications

Chemical Name	Chemical Formula	Vendor	Specifications
Mercury Chloride	$HgCl_2$	Sigma Aldrich	≥ 99.5%
Titanium Dioxide	TiO_2	Sigma Aldrich	≥ 99.5% trace metals basis
Sodium Hydroxide	NaOH	Fisher Scientific	≥ 97%
Hydrochloric Acid	HCl	VWR	12 M, 37%
Sodium Borohydride	$NaBH_4$	VWR	≥ 98% , J.T.Baker®

3.4 Surface Characterization of Solid Samples

The morphology and structure of all TiO_2 samples (nanoparticles and Ti-NT) were characterized by TEM (JEOL JEM-2010) and SEM (FEI Quanta 400 ESEM). For TEM analysis, the samples were suspended in methanol under sonication and then placed on a carbon film on 400-mesh copper grid (Electron Microscopy Science) for analysis.

For SEM analysis, a gold sputtering technique was followed where the TiO_2 samples were coated with gold to avoid the electric charging effect of the samples as a result of the analysis.

Surface elements of TiO_2 solid samples before and after treating mercury were analyzed by XPS (Kratos Axis Ultra DLD) with monochromatic Al Ka anode source (15 kV). High-resolution XPS spectra of O (1s), Ti (2p), and Hg (4f) were collected with 20 eV of pass energy and 10 times sweeps. The Hg (4f) spectra were deconvoluted using

XPSPEAK software program with Shirley background to quantify Hg species such as Hg(0), Hg (I), and Hg(II).

4. RESULTS AND DISCUSSION

4.1 Precision and Accuracy Test Results

Since CVAAS was the primary method for determining the mercury concentration, an initial step of conducting a precision and accuracy test was performed. Six solutions of 30 μg/L Hg(II) were prepared (Table 7) and analyzed using CVAAS as detailed in Section 3.1.4. Accuracy, also known as the closeness of a measured value to a standard or known one, was calculated by finding the average % recovery of the six samples. The % recovery was calculated by dividing the measured mercury concentration by the theoretical one. The results are summarized in Table 7.

Table 7: Accuracy and precision test results

Sample Number	Measured Mercury Concentration (μg/L)	% Recovery
1	31.6	105%
2	27.1	90%
3	31.0	103%
4	32.3	108%
5	28.6	95%
6	29.6	99%
Average	**30.0**	**100.1**

On the other hand, precision refers to the closeness of two or more measurements to one another. This was represented as the relative standard deviation:

$$Relative\ standard\ deviation = \frac{Standard\ deviation}{average} \times 100 = \frac{1.998}{30} \times 100 = 7\%\ (Precision) \quad (6)$$

Additionally, the method detection limit (MDL) of the CVAAS was calculated by multiplying the standard deviation by the student t-value at a confidence level of 99%. For a degree of freedom of 5 (Number of samples -1) with a 99% confidence level, the t-distribution value is 3.365 [81]. Using the calculated standard deviation and the related student t-value, the detection limit was calculated by multiplying the two measurements to obtain an MDL of 7 µg/L.

This limit represents the minimum value of mercury concentration that can be confidently measured using CVAAS. It is noteworthy to mention that throughout the entire experimentation and analytical testing, samples were diluted to approximately 30 µg/L (mid-way on the calibration curve) to avoid measuring anything less than the detection limit and beyond the maximum calibration standard, thereby increasing confidence in the reported data. Overall, these calculations show that both the preparation and analytical methodology is reliable to conduct accurate and precise analyses.

4.2 Surface Characterization of Materials

4.2.1 XRD Analysis

The crystal phases of the synthesized nanotubes were characterized by XRD. Figure 8 shows the obtained XRD patterns for Ti-NT compared with commercial P25 TiO_2. Published 2-theta values representing peaks for pure rutile and anatase forms of TiO_2 are listed in Table 8 [82]. These were used to identify the peaks generated in the XRD analysis (labelled as A (anatase) and R (Rutile) in Figure 8). An XRD image of commercial P25 TiO_2 found in the literature is illustrated in Figure 9. The peaks in Figure 9 seem to match the ones generated in this research (Figure 8).

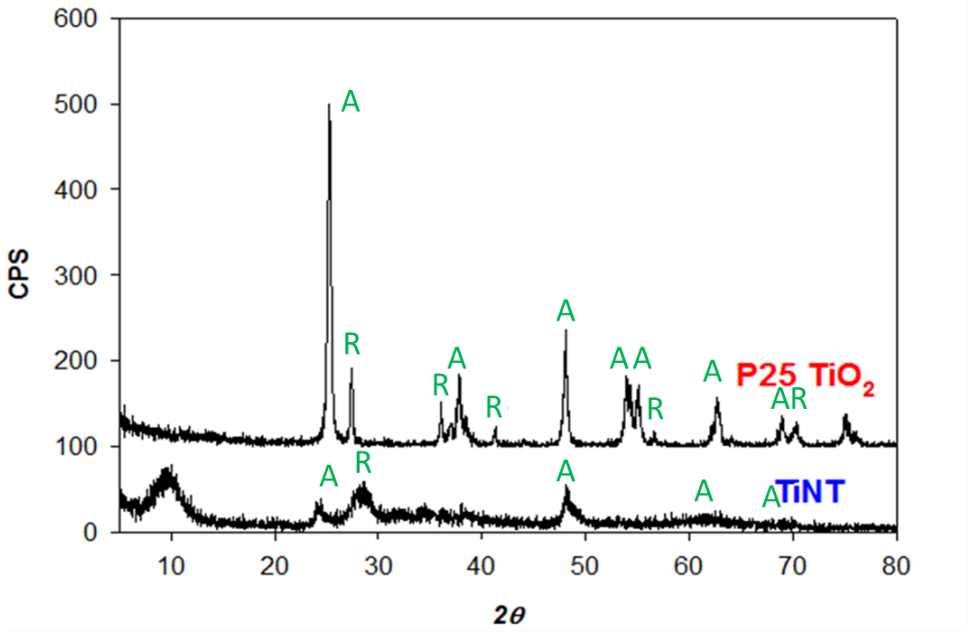

Figure 8: XRD patterns of Ti-NT and commercial TiO_2 nanoparticles

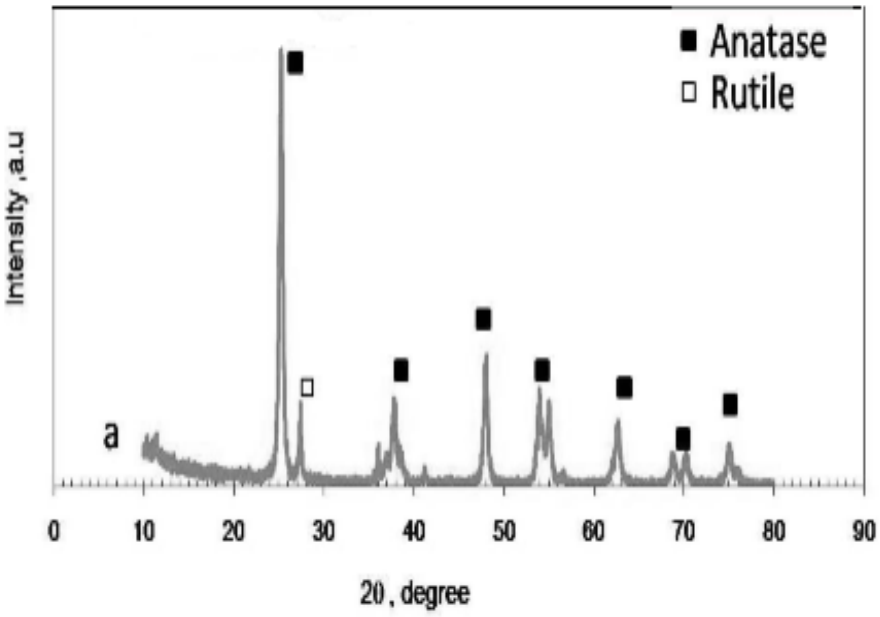

Figure 9: Published XRD results for P25 TiO_2 nanoparticles [83]

Table 8: 2-theta values for pure rutile and anatase forms of TiO_2 [82]

Titanium dioxide type	Anatase TiO_2	Rutile TiO_2
2θ	25.34, 37.81, 48.1, 53.92, 55.14, 62.75, 68.81	27.45, 36.09, 41.23, 54.32, 56.04, 69.01

It can be observed from Figure 8 that the XRD peaks of the nanotubes were broader and less intense than those of the nanoparticles. They were indexed to both anatase and rutile phases, meaning that hydrothermal treatment did not affect the form of the TiO_2 precursor. Although the material consisted of anatase and rutile, a reasonable amount of titanate structure was found to be formed after the treatment. The prominent titanate peak could be attributed to sodium titanate which is generally found at 2Θ value of 10 degrees [84].

Sikhwivhilu et. al also observed the formation of an additional peak at 2Θ degrees angle that was associated with a titanate structure. They also compared the formation of nanotubes hydrothermally using microwave digestion compared to the conventional autoclave method. Shorter peaks were observed for the rutile and anatase phases (35% and 41% respectively) compared to the P25 precursor (20% and 80% respectively) due to the formation of a titanate structure (24%). These XRD results match the ones found throughout this research [82].

Wu et al. conducted similar research to investigate the synthesis of titania nanotubes via microwave irradiation. However, they used chemical-pure (anatase) TiO_2 as a precursor to the hydrothermal formation of nanotubes. XRD analysis revealed the shortening of the anatase peaks after hydrothermal treatment. This was explained by the destruction of the crystalline structure of the raw materials as a result of microwave irradiation [72]. On the other hand, results from Sikhwivhilu et al.'s comparison of conventional hydrothermal treatment to microwave digestion found that the crystallinity of the sample synthesized using microwave irradiation was better than that the one

prepared by conventional heating as shown in the XRD results (Figure 10). Possible reason for this could be the shorter reaction time for microwave processing [82].

As for the peak broadening that was caused by the hydrothermal treatment, it was reported in the literature that this could be as a result of the crystal size and curvature of the nanotubes [85]. The small crystal size of the nanotubes resulted in broadened reflections in the XRD pattern due to the small coherence area value. Additionally, the scrolling of the nanotube along the crystallographic axis could also result in peak broadening. The curvature of the nanotube could also affect the crystal unit cell due to bond bending. This could lead to variations in the peak intensity of the XRD results. Another factor that could influence peak deterioration is the energy and intensity of the electron beam utilized in the electron diffraction and imaging technique [85].

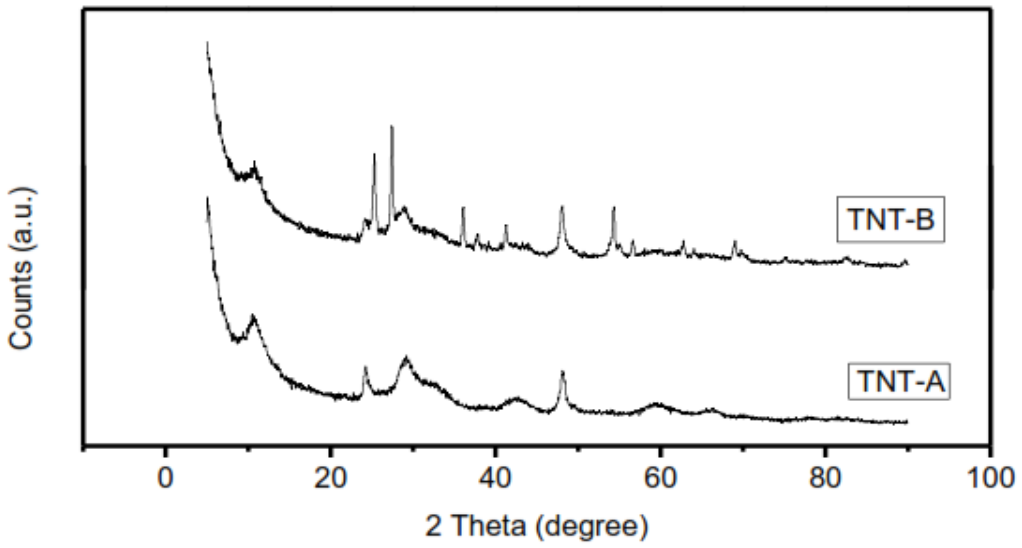

Figure 10: XRD results comparing Ti-NT prepared hydrothermally by autoclave (TNT-A) and microwave irradiation (TNT-B) as reported in literature [82]

4.2.2 TEM Analysis

TEM images of TiO_2 before and after hydrothermal treatment are depicted in Figure 11. Results show that the hydrothermal method was successful in transforming the almost-spherical nanoparticles into the desired nanotubes with a mean diameter and length of approximately 10 nm and 350 nm, respectively. The size of the precursor nanoparticles ranged from 10 to 60 nm with an average diameter of 30 nm. This was found to be similar to the reported primary particle size of 21 nm as stated by the manufacturer (Sigma Aldrich).

Microwave digestion reaction took place in 60 minutes at 1,600 W power. Reported length and diameter values for hydrothermally synthesized nanotubes are within the range of 100-1000 nm and 7-12 nm, respectively; validating the results that are obtained by this research [79, 85]. According to TEM results, the nanotubes appeared amorphous and their walls created a contrast in the image, revealing that they possessed an internal structure.

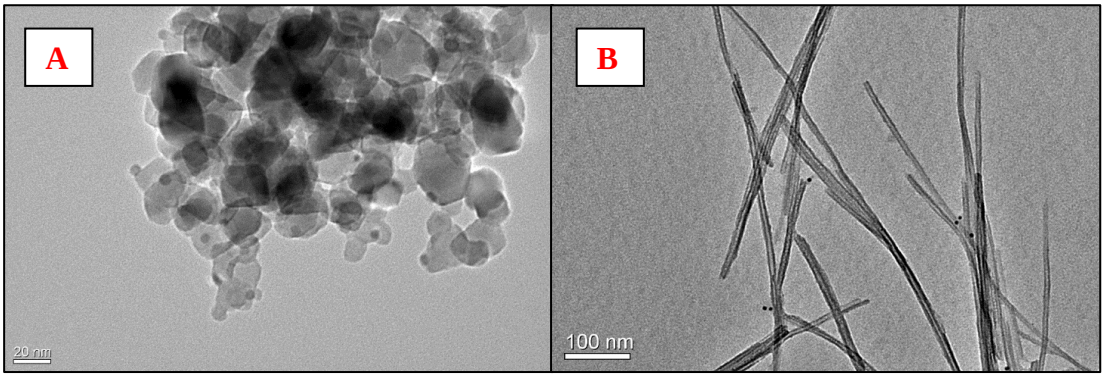

Figure 11: TEM images of TiO_2 before (A) and after (B) hydrothermal treatment

4.2.3 SEM Analysis

Figures 12 and 13 show the obtained SEM images of commercial Sigma Aldrich P25 TiO_2 and Ti-NT respectively. Figure 13A depicts many fiber-like nanotubes extending from the nanosized TiO_2. Published SEM results show similar observations (Figure 14). [63] The SEM analyses, coupled with the TEM images shown in Section 4.2.2, indicate that the wire-like structures observed in Figure 13 are nanotubes, thereby supporting that hydrothermal treatment via microwave irradiation produces titanium dioxide nanotubes.

Ti-NT produced from the nanopowder exhibit larger surface area, therefore enhancing the efficiency of electron transport and the separation of electron-hole pairs, leading to greater photocatalytic activity [63].

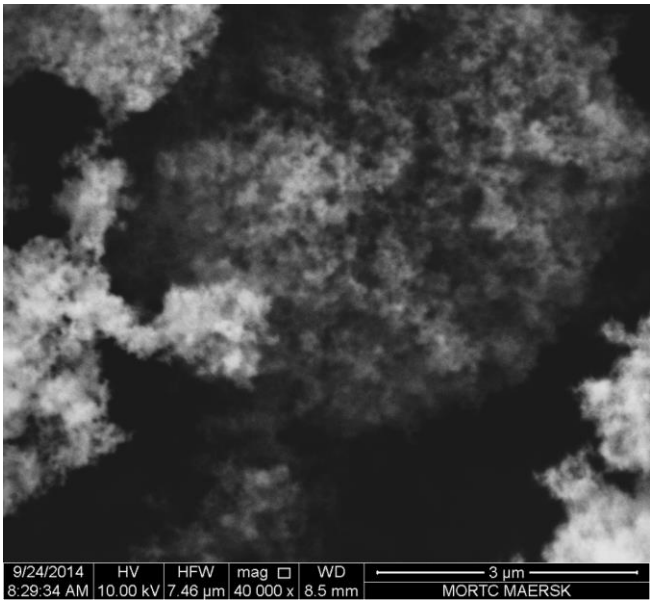

Figure 12: SEM image of Sigma Aldrich P25 TiO_2 nanoparticles

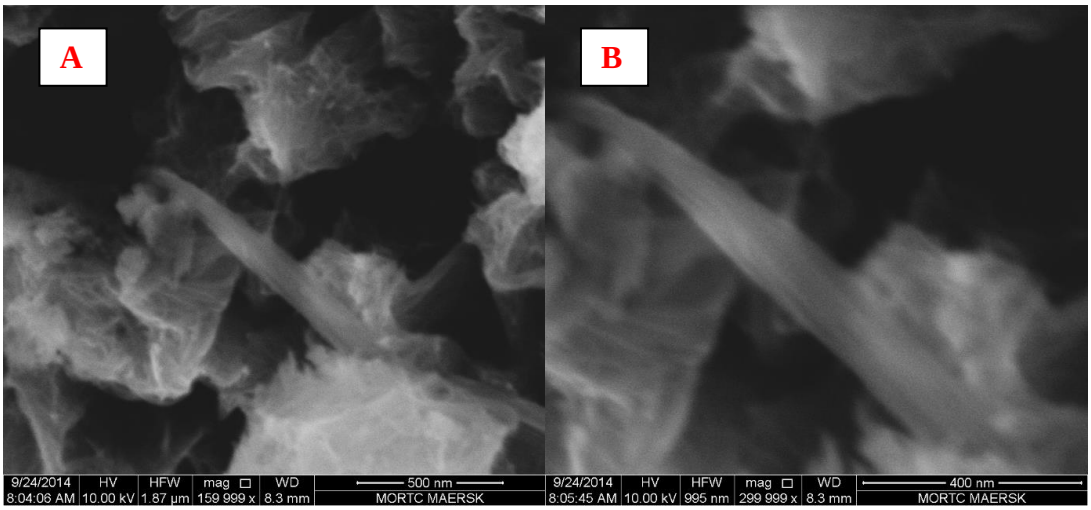

Figure 13: SEM images of Ti-NT produced from P25 nanoparticles precursor at (A) 160,000 and (B) 300,000 magnification

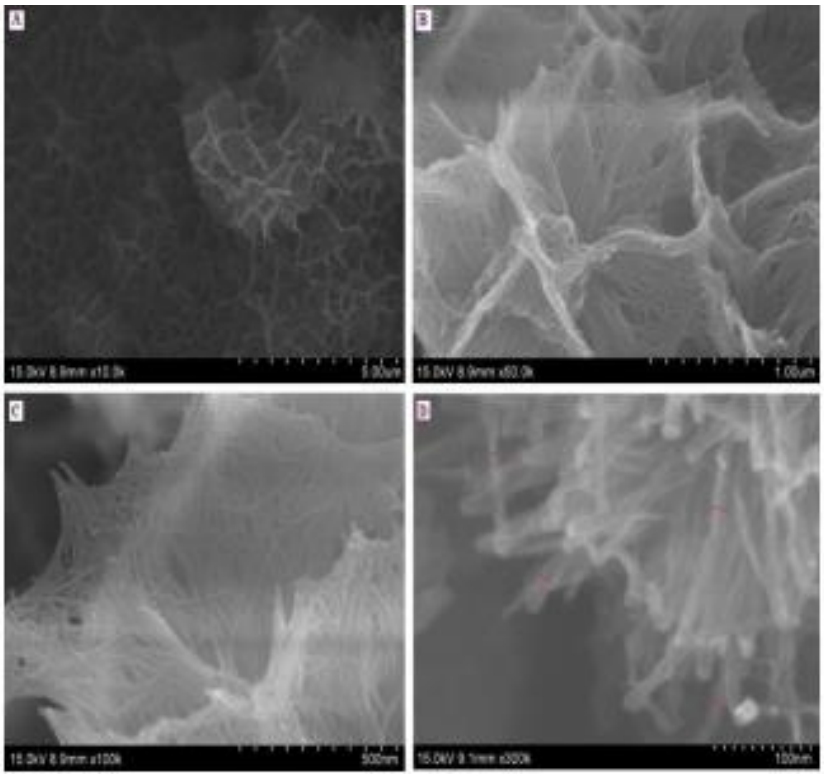

Figure 14: Published results for SEM images of Ti-NT at (A) 10,000 (B) 50,000 (C) 100,000 and (D) 300,000 magnification [63]

4.2.4 XPS Analysis

Limited data are available in the literature for the application of XPS to examine Ti-NT. However, it has been used to evaluate other forms of TiO_2, especially in cases where the material was doped. Although XPS is commonly used for surface analysis, it is primarily a bulk method in the examination of nanotubes since the sampling depth is greater than the nanotube's cross-section. Therefore, it has an advantage of determining the nanotube's phase in addition to its composition [85].

In TiO_2, both Ti^{4+} and O^{2-} peaks could be seen at their expected binding energy levels. Deviation of the binding energies from the typical values may be due to bond enviornment changes, such as bond strengthening or weaking, depending on the conditions. Reported Ti ($2p_{3/2}$) binding energies for sodium titanate and TiO_2 are 458.1 and 458.9 eV, respectively [85]. As for O (1s) binding energies in TiO_2, reported values range from 529.7-530.2 [86]. The resolution of XPS and its sensitivity were found to be high enough to measure the small energy difference between the two materials (sodium titanate and TiO_2). Despite the small shift between the two, it was sufficient to represent the strengthening and shortening of the Ti-O bond in the titanate structure relative to the TiO_2 [85].

Similar results for both Ti ($2p_{3/2}$) and O (1s) were observed in the present study where XPS analysis were conducted on the precursor P25 nanoparticles and the hydrothermally synthesiszed Ti-NT. The intensity of the nanotubes' major Ti ($2p_{3/2}$) peak was found to be lower than that of the nanoparticles. This can be explained by the presence of both titanate and titanium dioxide in the nanotubes' as a result of

hydrothermal treatment, validating the XRD results presented in Section 4.2.1. Detailed spectra are depicted in Figures 15 and 16 and the major peaks are summarized in Table 9.

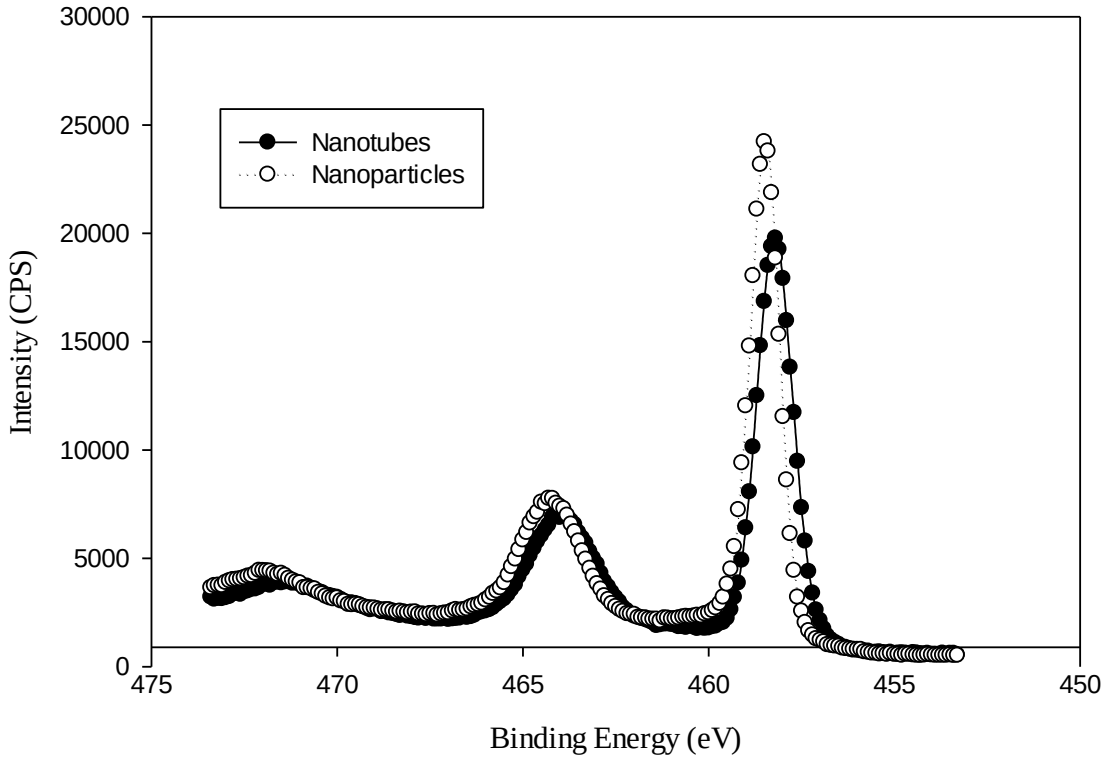

Figure 15: Ti ($2p_{3/2}$) XPS results for TiO_2 nanoparticles and hydrothermally synthesized Ti-NT

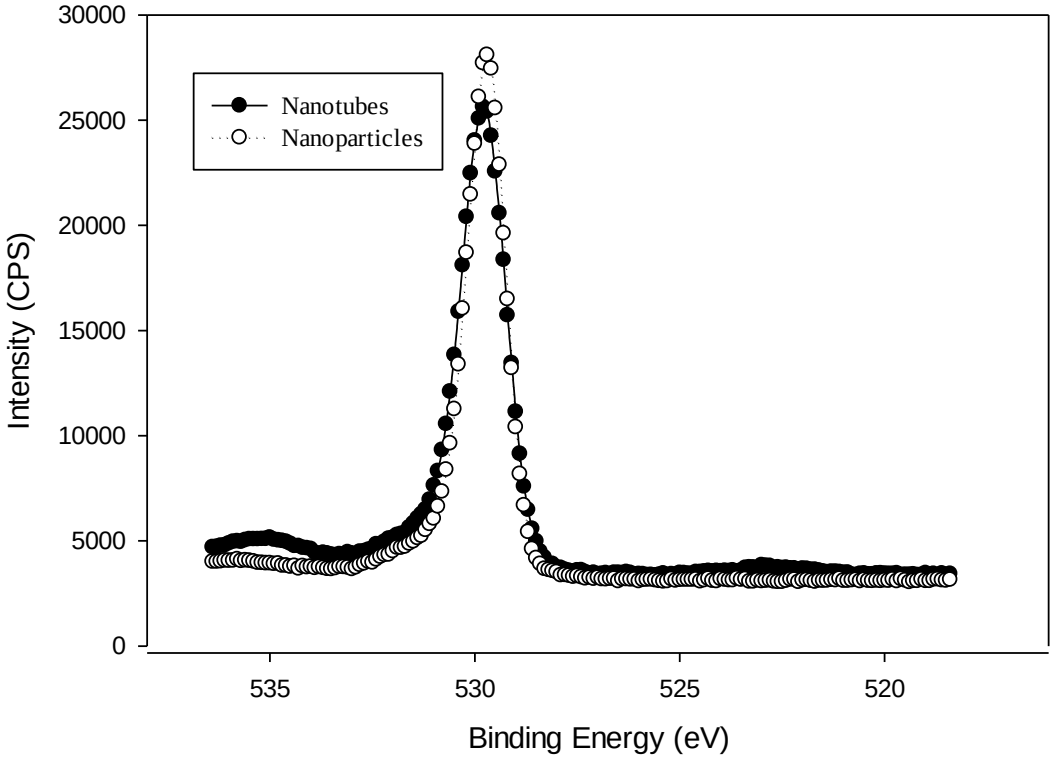

Figure 16: O (1s) XPS results for TiO_2 nanoparticles and hydrothermally synthesized Ti-NT

Table 9: Ti-NT and TiO_2 nanoparticles' binding energies from XPS analysis

TiO_2 Morphology	Ti ($2p^{3/2}$) Binding Energy (eV)	O (1s) Binding Energy (eV)
Nanotubes	458.2	529.9
Nanoparticles	458.5	529.8

4.3 Mercury Removal from Aqueous Solutions

Experiments of mercury (II) removal from aqueous solutions were performed in the dark and under simulated sunlight irradiation at different conditions. These conditions included different photocatalyst dosages, pH values, concentrations of added hole scavenger (formic acid), and different types of photocatalyst (TiO_2 particles and nanotubes).

4.3.1 Adsorption of Hg(II) onto TiO_2

In order to differentiate photocatalytic chemical reduction of Hg(II) from physical adsorption, experiments were carried out in the dark using a solution of 1 mg/L Hg(II) ($HgCl_2$) at different pH levels and photocatalyst dose. Table 10 lists the Hg (II) adsorption percentage at different concentration and type of photocatalyst and different pH levels. The initial mercury concentration in these experiments was 1 mg/L. The percent removals were calculated after 2 hours of contact time.

Table 10: Percentage removal of Hg(II) by adsorption at different conditions

Photocatalyst type	Photocatalyst dose	pH	% Hg Removal
Nanoparticles	1 g/L	4	2%
Ti-NT	0.1 g/L	4	70%
Ti-NT	0.01 g/L	4	31%
Ti-NT	0.01 g/L	10	98%

To study the effect of pH, an experiment with 0.01 g/L Ti-NT was performed at pH levels 4 and 10. As shown in Table 10, the adsorption of Hg(II) on TiO_2 strongly depended on the solution pH; showing increased removal at alkaline pH levels. Hg(II) showed less affinity for Ti-NT at pH 4 than it did at pH 10 with a % removal of 31% and 98%, respectively.

Table 11 summarizes published data regarding Hg(II) adsorption on titanium dioxide at different conditions. Although the published values are primarily affiliated with commercial titanium dioxide, the trends could be used for comparison purposes with the present results that were associated with the nanotubes.

When comparing the present findings to those found in the literature, discrepancies in the % Hg(II) removal results were found. This can be attributed to different experimental conditions and analysis techniques. However, all those results show the same trend: increasing solution pH causes more Hg(II) to adsorb on the photocatalyst surface, therefore enhancing the Hg(II) removal. The trend can be explained by the surface chemistry (of both mercury and TiO_2) and its dependence on the solution pH.

Table 11: Published data for Hg(II) removal by adsorption on Degussa P25 TiO_2

Author	pH	[TiO2]: [Hg(II)]	% Hg Removal
Wang et al. [30]	2.5, 3, 4	17.9	2, 5, 12
Botta et al.[87]	3, 11	10.0	15, 25
Serpone et al.[88]	5, 7	20.0	30, 90
Chen et al.[89]	7	16.7	10
Khalil et al. [6]	4	20	31

Electrophoretic mobility is one of the most efficient techniques for surface charge investigation of metal oxide solutions. This method quantifies the migration of suspended particles under an electric field. The isoelectric point (pI) of the titanium dioxide depends on the alkali-acid character of the surface hydroxyl groups. At the pI, no excess surface charges are present on the titanium dioxide, thereby minimizing the electrostatic interaction.

The dissociation reactions of the surface hydroxyl groups depend on the pH levels, and the oxide acidity can be related to dissociation constants of the reactions. For instance, at pH levels lower than the pI, protonated surface species of TiO_2 ($\equiv Ti\text{-}OH_2^+$) can form (Equation 7) and the surface is positively charged. On the other hand, at pH levels greater than the pI, the surface of TiO_2 is deprotonated with negatively charged species of $\equiv Ti\text{-}O^-$. (Equation 8). The lower the isoelectric point, the higher the concentration of hydroxide ions of the TiO_2 surface [6]. Reported isoelectric point values (pI) for commercial titanium dioxide Degussa P25 are between 6.8-7. [10, 30]. As for the titanium dioxide nanotubes, literature reports pI values between 5.3-5.5 [90].

At acidic conditions (pH 4), TiO_2 particles are positively charged according to the equilibrium equation (Equation 7):

$$\equiv Ti - OH + H^+ \leftrightarrow \equiv TiOH_2^+ \quad (7)$$

At basic conditions (pH 10), $\equiv TiO^-$ groups are the prevalent species as a result of the deprotonation of the surface hydroxyl groups above the pI [10]:

$$\equiv Ti - OH + OH^- \leftrightarrow \equiv TiO^- + H_2O \ (8)$$

Therefore, more electrostatic attraction between the positively charged mercury species and the negatively charged TiO_2 surface occurs at basic conditions. Therefore, the amount of mercury adsorbed increased at higher pH values.

Table 10 indicates that more adsorption is shown using the nanotubes as compared to the nanoparticles. This is not only due to the higher surface area of the nanotubes than the nanoparticles [72, 91] but also to the lower charge density on the surface of the nanotubes (average pI of 5) as compared with the nanoparticles (average pI of 7) at the same pH [30].

Table 10 also compares the amount of Hg(II) adsorbed on Ti-NT using two different Ti-NT doses (0.01 g/L and 0.1 g/L Ti-NT). As expected, the higher the concentration of titanium dioxide, the more Hg(II) is adsorbed. This can be explained by the increased amount of surface sites available with higher titanium dioxide concentrations.

One of the methods of evaluating the ability of sorbent to remove a certain contaminant is to determine the distribution coefficient, K_d (mL/g) [4]. This value is

defined as the ratio of the quantity of a material adsorbed (Hg(II)) per unit mass of solid (TiO_2) to the amount of adsorbate remaining in solution at equilibrium as shown in Equation 9.[92] For the purpose of this study, the lab-scale batch method was utilized to determine the K_d values.

$$K_d = \frac{(C_{in} - C_f)}{C_f} r_{ws} \quad (9)$$

Where C_{in} is the initial metal (Hg(II)) concentration (mg/L); C_f is the final metal (Hg(II)) concentration (mg/L); and r_{ws} is the ratio of water to solid (titanium dioxide) (mL/g) [93].

High K_d values indicate an enhanced ability of the sorbent to retain a particular species. Generally, when the K_d value exceeds 1,000, then the material is a good sorbent. Values that are 10^{+4} or higher are considered exceptional [94]. Table 12 summarizes K_d values for titanium dioxide (both nanotubes and nanoparticles) at different concentrations and solution pH levels.

Table 12: K_d values at different conditions

Photocatalyst type	Photocatalyst dose	pH	K_d values
Nanoparticles	1 g/L	4	2.6E+01
Ti-NT	0.1 g/L	4	1.2E+04
Ti-NT	0.01 g/L	4	2.2E+04
Ti-NT	0.01 g/L	10	2.2E+06

The K_d values for the nanotubes were larger by three orders of magnitude as compared to the nanoparticles, meaning that the nanoparticles were less efficient Hg(II) sorbents than the nanotubes. The performance of Ti-NT was exceptional with K_d values as large as 10^6. Scarce information regarding K_d values are found in the literature for the application of Ti-NT for Hg(II) removal. However, data with the use of TiO_2 nanoparticles as a sorbent for the removal of mercury and other metals (lead, cadmium and nickel) can be used to place current findings in perspective.

Dou et al. reported K_d values of 119.5 and 140.5 when using TiO_2 nanoparticles (prepared by hydrolysis and sol-gel methods respectively) to remove Hg(II) from water in the dark [4]. These values are almost of the same order as that calculated in this study. Differences could be attributed to the nanoparticle preparation method or experimental/ analytical differences. When TiO_2 was investigated for the adsorption of lead, cadmium, and nickel, K_d values of 10^7, 10^5 and 10^4 were reported, respectively. The experiments were conducted at pH 8 using commercial TiO_2 nanoparticles from Sigma Aldrich [93]. These results show that values as high as 10^6 are realistic for TiO_2.

In summary, Ti-NT showed an excellent adsorption capacity as compared to the nanoparticles. This made the nanotubes a viable method of removing Hg(II) from water. However, they still maintain the disadvantage that mercury is present in the salt form as opposed to the elemental one. Therefore, this research was taken a step further to investigate the photocatalytic removal of Hg(II) to convert it to elemental mercury using photocatalysts under solar light.

4.3.2 Photocatalytic Removal of Hg(II)

4.3.2.1 Effect of Irradiation Time and Photocatalyst Dosage

Figure 17 illustrates results of the Hg(II) photoreduced by irradiation as a function of time at pH 4, where the pH was adjusted using 3M HCl acid. The amount of Hg(II) that was photoreduced increased with increasing irradiation time until the system reached equilibrium after thirty minutes. In the presence of 0.01 g/L and 0.1 g/L Ti-NT, 62% and 99% of mercury (II) were removed, respectively.

An additional experiment was performed using 0.05 g/L Ti-NT to address the effect of varying photocatalyst dosage on the photocatalytic reduction of Hg(II). Results after 30 minutes of irradiation are summarized in Table 13. As expected, both the amount of Hg(II) consumed during the reaction and the reaction rate increased with increasing Ti-NT concentrations. In a solution with constant amount of reagents, increasing the catalyst concentration causes more active sites to be available and increases the interception of UV radiation by the particles, thereby enhancing Hg(II) adsorption that ultimately leads to more photoreduction to occur. Similar observations

were reported by Assadi et al. and Mitra et al. in their research of reducing hexavalent chromium using zinc oxide photocatalyst [95, 96].

Although heterogeneous photocatalytic degradation reactions are known to increase with catalyst loading, excess catalyst causes unfavorable light scattering and reduction of light penetration into the solution. Therefore, since the reaction time of Hg(II) photoreduction is known to be 30 minutes, 0.1 g/L of Ti-NT seemed to be an adequate concentration since it resulted in almost complete Hg(II) removal at the given conditions [97].

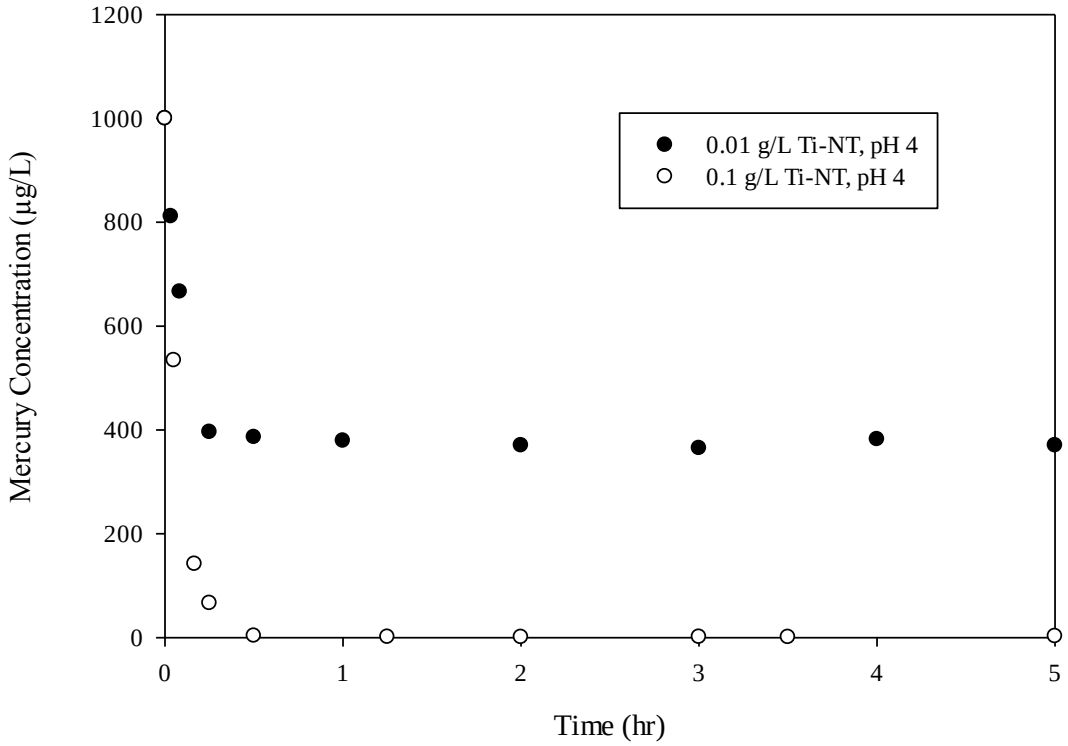

Figure 17: Kinetics of Hg(II) removal with varying Ti-NT concentrations

Table 13: % Mercury removal at various Ti-NT concentrations

Ti-NT Concentration (g/L)	% Mercury Removal (%)
0.01	62
0.05	80
0.1	99

4.3.2.2 Effect of Nanotube Preparation Methodology

Experiments were conducted at similar conditions while varying the nanotube preparation methodology; in the first method (Method 1), the nanotubes were dried and grinded. In the second method (Method 2), the nanotubes were used in a solution with known concentration (20.5 g/L) without drying. Two experiments were conducted under the same conditions but with different types and concentrations of TiO_2; 1 g/L and 0.1 g/L of Ti-NT were used from Method 1 and Method 2 respectively. The solution pH was fixed at 4 and the initial Hg(II) concentration added was 1 mg/L. These experiments were repeated under the same conditions but with the addition of 2.5 mM formic acid.

After thirty minutes of irradiation time, 95% of the Hg(II) was removed using 1 g/L of the nanotubes prepared following Method 1 whereas >99.9% was removed using 0.1 g/L nanotubes prepared by Method 2 (Table 14). Ten times less nanotube dose was adequate to achieve similar removals when a suspension was prepared. This is because drying the nanotubes caused them to agglomerate, thereby decreasing the surface area available for Hg(II) to be adsorbed.

The addition of 2.5 mM formic acid did not make a significant difference to the performance of the nanotubes; For instance, those prepared by Method 1 removed 2%

more than the solution with no formic acid. No difference was observed in the experiments that used nanotubes from Method 2 (Table 14). The effect of formic acid on the efficiency of Hg(II) reduction will be discussed in more detail in Section 4.3.2.4. Since Method 2 deemed more efficient than Method 1, all the nanotubes that were used in the remainder of this study were prepared following Method 2.

Table 14: Effect of nanotubes preparation method on Hg(II) removal from solution

% Hg(II) Removal	Without Formic Acid	With 2.5 mM Formic Acid
Method 1 (1g/L Ti-NT)	95%	97%
Method 2 (0.1 g/L Ti-NT)	>99.9%	>99.9%

4.3.2.3 Effect of pH on Hg(II) Photoreduction

As a control test, a blank experiment with 1 mg/L Hg(II) without titanium dioxide was conducted under irradiation of 1 Sun. Results showed no decrease in Hg(II) concentration over the course of four hours. This shows that all Hg(II) removal is attributed to the addition of TiO_2.

According to Section 4.3.1, Hg(II) adsorption on TiO_2 was evaluated in the dark to clearly distinguish between the photocatalytic Hg(II) reduction and the removal by adsorption. Also, based on the results in Table 10, a Ti-NT concentration of 0.01 g/L was used when evaluating the effect of other parameters on Hg(II) removal. The experiments were performed in atmospheric conditions. Although published data show that the absence of oxygen enhances the process, this research focused on optimizing the Hg(II) removal without having to maintain anoxic conditions [6].

Figure 18 illustrates the results of Hg(II) photo-reduced as a function of time at different solution pH values in the presence of Ti-NT. Increasing the solution pH slightly enhanced photo-reduction of Hg(II) with time.

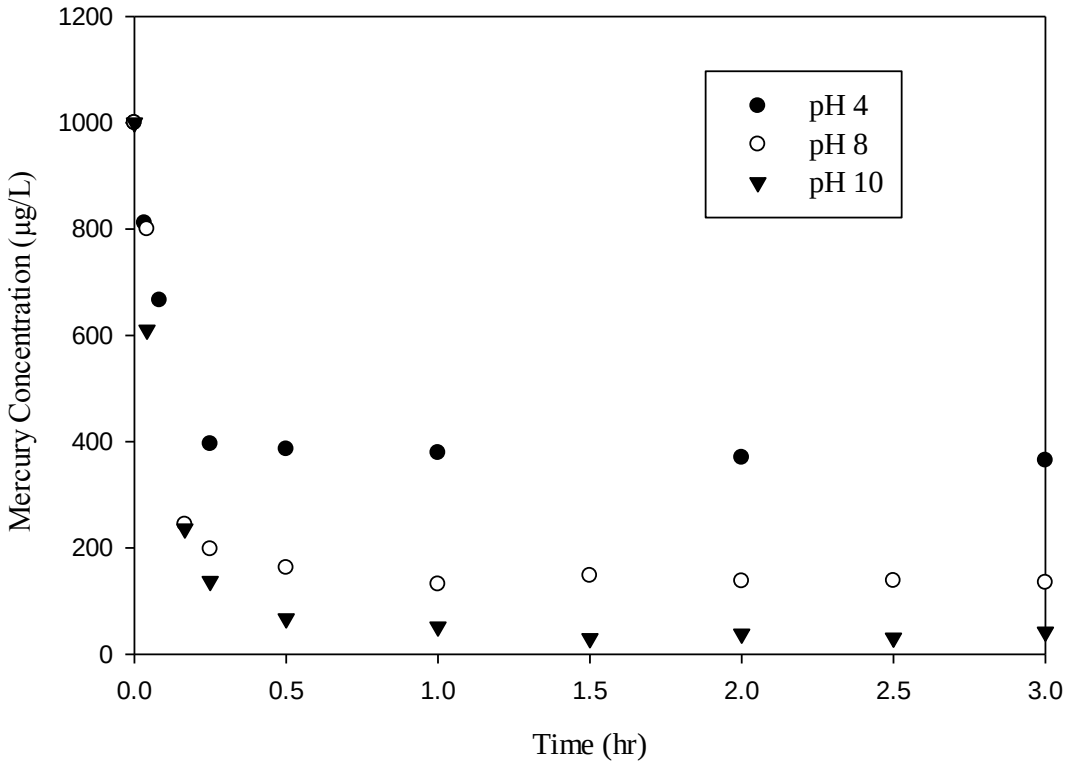

Figure 18: Effect of pH on Hg (II) photo-reduction using 0.01 g/L Ti-NT

The change in kinetics of Hg(II) reduction as a result of varying the solution pH can be explained by the following factors:

i. Potential level of TiO_2's conduction band

ii. The redox potentials of the various mercury species present at the different pH solutions

iii. Hg(II) adsorption at different pH levels

The conduction band potential (E_{CB}) of TiO_2 depends on the pH of the solution, shifting to more cathodic potentials by 59 mV per pH unit (Equation 10) [10]:

$$E_{CB} = -0.05 - 0.059pH\ (at\ 25^oC) \quad (10)$$

Therefore, the driving force of the electrons in the conduction band increases as pH increases [10] Table 15 lists the calculated E_{CB} values for titanium dioxide at pH 4, 8 and 10. [98]

Table 15: Conduction band potential of titanium dioxide at various pH levels

pH	4	8	10
E_{CB}	-0.286	-0.522	-0.64

The relation between the redox level of metallic couples to the levels of the conduction band is probably the single most important parameter to predict feasibility of the species reduction; the higher the standard reduction potential of a particular species and the more positive the potential of a species, the higher its tendency to be reduced [61]. Table 16 summarizes the standard potentials for reduction of $HgCl_2$, Hg_2Cl_2 and

$Hg(OH)_2$. No literature data is found for HgClOH [10]. Clearly, the most positive potential is for the element $Hg(OH)_2$, which is present at more basic pH solutions (Figure 2).

Table 16: Standard reduction potentials for various mercury species

Mercury Species, Reaction	E^o
$Hg(OH)_2 + 2H^+ + 2e^- \rightarrow Hg^0(l) + 2H_2O(aq)$	1.034
$2HgCl_2 + 2e^- \rightarrow Hg_2Cl_2 + 2Cl^-(aq)$	0.63
$HgCl_2 + 2e^- \rightarrow Hg^0(l) + 2Cl^-(aq)$	0.41
$Hg_2Cl_2 + 2e^- \rightarrow 2Hg^0 + 2Cl^-(aq)$	0.268

The greater photocatytic reduction for Hg(II) obtained at pH values of 8 and 10 as compared to pH 4 is due to the higher driving force of the conduction band electrons, the thermodynamic feasibility for $Hg(OH)_2$ reduction to elemental mercury which has the highest redox potential and it is present at basic pH conditions, in addition to the enhanced adsorption of Hg(II) at higher pH levels as seen in Section 4.3.1 [10].

To further explain the importance of adsorption on the photocatalytic reduction of Hg(II), the overall process of photocatalytic removal has to be studied. In summary, the process consists of the following steps, where the photocatalytic reduction of Hg(II) occurs in the adsorbed phase [4]:

i. Transfer of the reactants in the fluid phase to the surface
ii. Adsorption of the reactants

iii. Photocatalytic reaction in the adsorbed phase

iv. Desorption of the products

v. Removal of the products from the water-solid interface regions

4.3.2.4 Effect of Formic Acid on the photocatalytic reduction of Hg(II)

Formic acid (FA) was selected to be the sacrificial electron donor of choice to study the effect of organic additives on the photocatalytic reduction of Hg(II). A control test was performed with a solution of 2.5 mM FA and 1 mg/L Hg(II) without titanium dioxide or sunlight irradiation. Results showed negligible Hg(II) decrease upon the addition of formic acid, meaning that Hg(II) does not complex with FA and the presence of FA does not interfere with Hg(II) analysis. Published results also agree that the addition of FA does not significantly affect the adsorption rate of Hg(II) on TiO_2 [10].

Experiments were performed with two different Ti-NT concentrations (0.01 g/L and 0.1 g/L) and two concentrations of FA were investigated: 0.25 mM and 2.5 mM. Figure 19 illustrates the time course of Hg(II) reduction in the presence and absence of formic acid. 3M HCl solution was used to adjust the pH to 4 in the case where no FA was added. The % mercury removals after 30 minutes irradiation time are also summarized in Table 17.

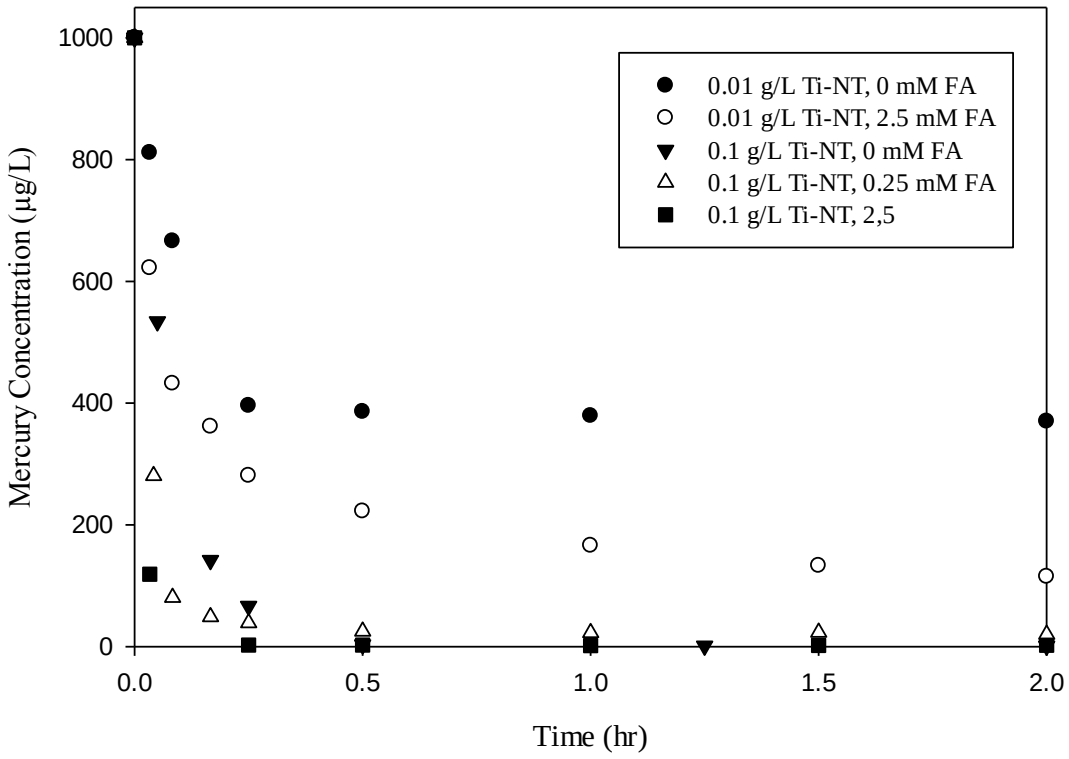

Figure 19: Effect of Formic acid on photocatalytic reduction of Hg(II) at pH 4 using different concentrations of Ti-NT

Table 17: % Hg removal at different formic acid concentrations

Ti-NT Concentration (g/L)	Formic Acid Concentration (mM)	% Hg Removal
0.01	0	62%
0.01	2.5	78%
0.1	0	99%
0.1	0.25	98%
0.1	2.5	99%

Results revealed that the addition of FA increased both the amount of Hg(II) reduced at pH 4, and the rate at which the reduction occurred. At 0.01 g/L of Ti-NT concentration, the addition of FA enhanced photocatalytic removal by almost 15%. The rate of reaction also increased upon the addition of FA. When 0.1 g/L of Ti-NT was used, almost all the Hg(II) was removed with and without FA addition. However, it can be seen that the reaction rate increased with increasing concentration of FA.

Furthermore, additional experiments were performed to study the extent at which the nanotubes could remove Hg(II) with and without the addition of FA. In those experiments, instead of adding 1 mg/L Hg(II) at the start of the testing, the solution was spiked with 1 ppm Hg(II) every 30 minutes, while maintaining the initial concentrations of FA and Ti-NT. In those experiments, 0.1 g/L Ti-NT were used since less concentrations failed to completely remove Hg(II) from the solution. The initial pH was adjusted at pH 4 using 3M HCl solution for the experiment that was conducted without FA. 2.5 mM FA was used in the other experiment and no pH adjustment was made. Results are depicted in Figures 20 and 21.

Figures 20 and 21 show that initial Hg(II) levels increased after each spike due to mercury accumulation from previous cycles. When FA was added, almost all of the added Hg(II) was removed at each cycle.

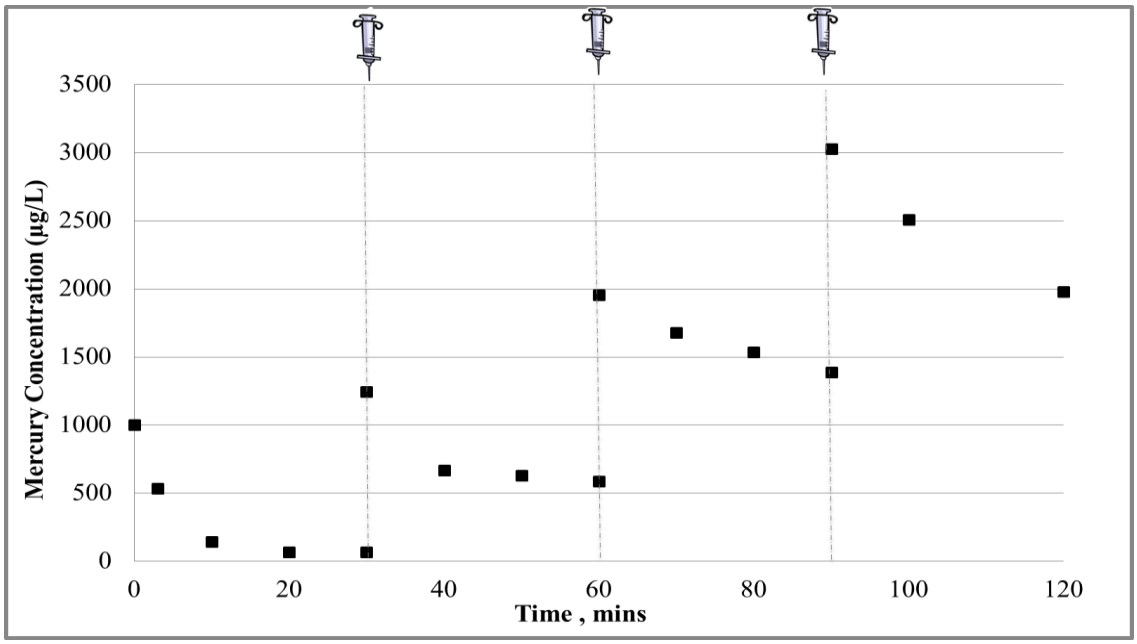

Figure 20: Continuous experiment without FA addition

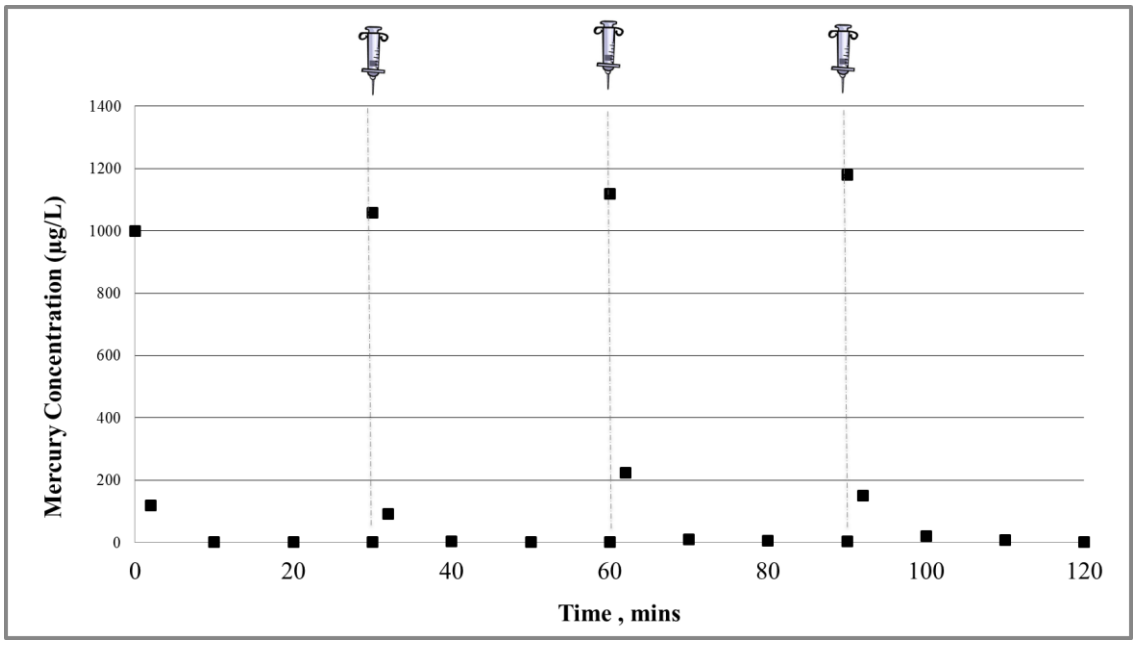

Figure 21: Continuous experiment with 2.5 mM FA addition

One of the primary factors that influence the efficiency at which photocatytic reduction occurs is the interfacial electron-transfer rate and the recombination lifetime of the valence band holes and conduction band electrons. To enhance the efficiency of the process, the recombination rate of the holes and electrons have to be minimized. In other words, maximizing the recombination lifetime of the holes and electrons. This can be achieved by filling the valence band holes by the electrons of a hole scavenger, such as FA in this case. In the absence of the electron-rich organic species, photo-generated holes would have to be filled by water following the pathway displayed in Equation 11. However, this four-electron-pathway reaction is a kinetically slow process.

$$2H_2O + 4h_{vb}^{+} \rightarrow O_2 + 4H^{+} \quad (11)$$

Where h_{vb}^{+} are the valence band holes [30].

The enhancement of the photocatalytic reduction of Hg(II) upon the addition of formic acid may be due to several reasons. First, the hydroxyl radicals formed in the photocatalytic process could react with formic acid and oxygen in the solution to produce superoxide, which further increases the process reaction [30]. Second, the water formed during the photocatalytic oxidation process redistributes the formic acid adsorbed on titanium dioxide from less active to more active sites, enhancing degradation rate of Hg(II) [99].

Since all the experiments were conducted in an open atmospheric condition, oxygen present in the solution is expected to compete with Hg(II) for conduction band electrons. The reason being that the rate constant for oxygen (equation 12) is somewhat higher than that of the Hg(II) reaction (equation 13). Therefore, it is expected that by

performing the experiments in anaerobic conditions, a higher removal rate for ions can be achieved. However, this is out of the scope of this study and is considered as a future extension to this work (Section 6).

$$O_2 + e_{aq}^- \rightarrow O_2^{\circ -}, k = 1.9\ x\ 10^{10}\ lmol^{-1}s^{-1} \quad (12)$$

$$Hg(II) + e_{aq}^- \rightarrow Hg(I), k = 7.1\ x\ 10^{9}\ lmol^{-1}s^{-1} \quad (13)$$

4.3.2.6 Effect of titanium dioxide photocatalyst type: nanoparticle vs. nanotube

To study the effect of the photocatalyst type on the photocatalytic reduction of Hg(II), kinetic experiments were performed at pH 4 with 1 mg/L initial mercury concentration while varying the concentration and type of TiO_2, and adding FA. Results are summarized in Figures 22 and 23.

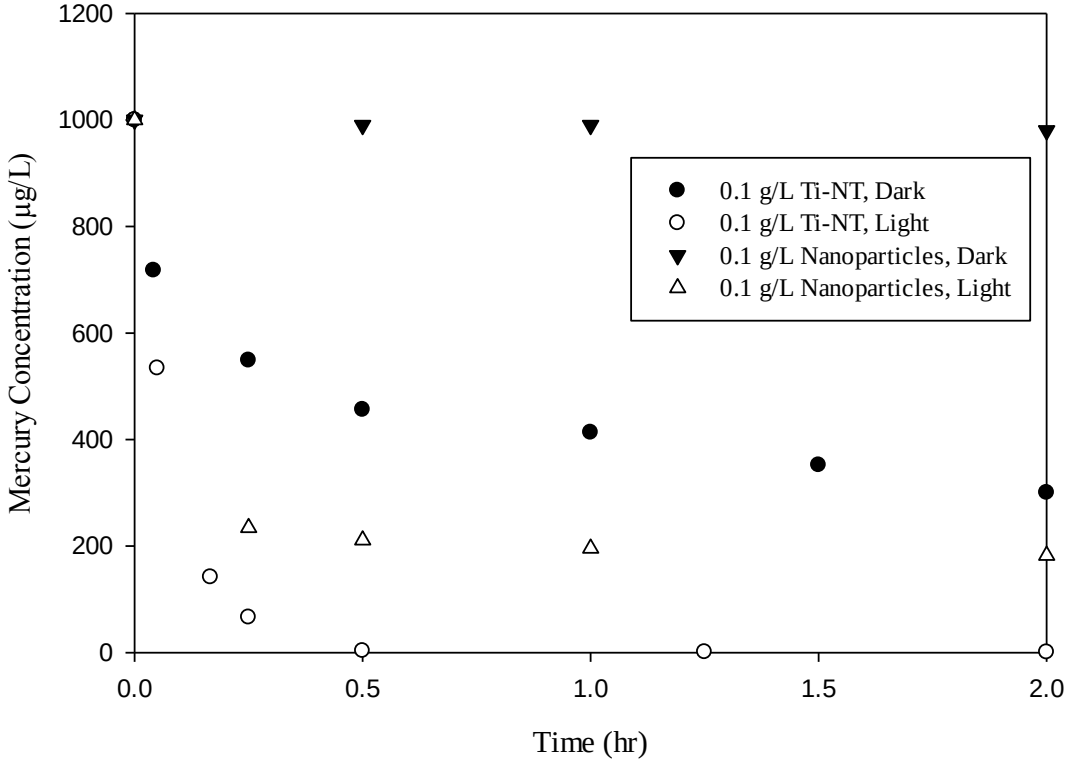

Figure 22: Kinetics of Hg(II) removal (dark and light) using 0.1 g/L Ti-NT and TiO_2 nanoparticles

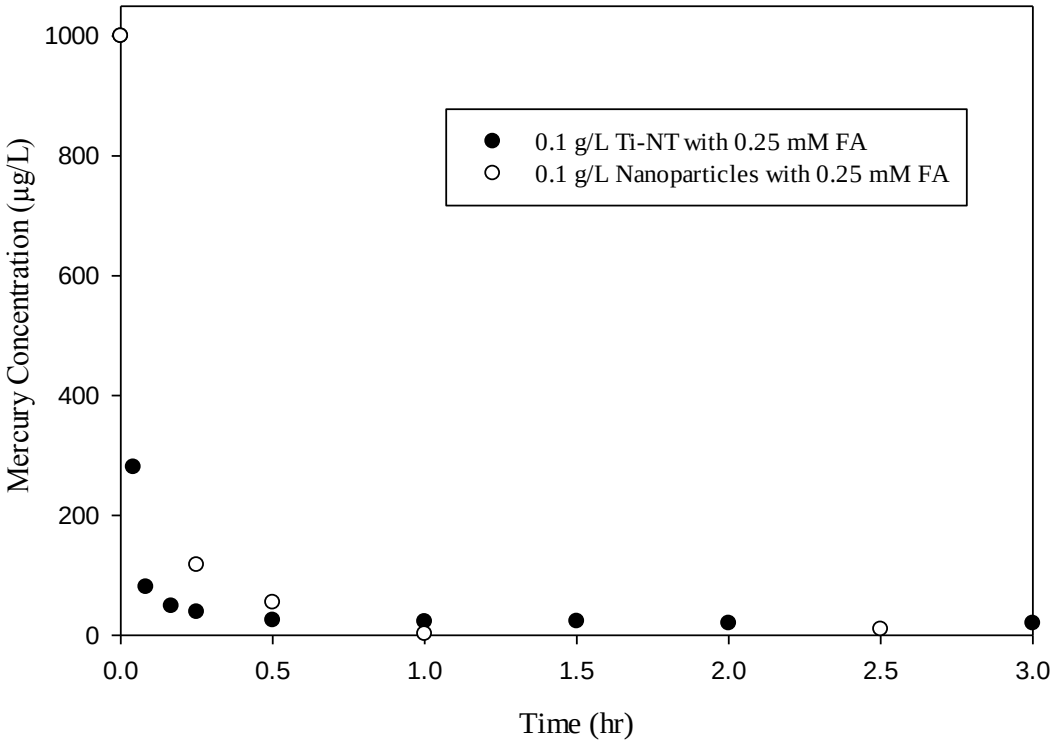

Figure 23: Kinetics of Hg(II) removal using 0.1 g/L Ti-NT and nanoparticles in a solution of 0.25 mM FA

As discussed in Section 4.3.2.1, it can be seen that the system achieved equilibrium after 30 minutes of reaction time. Figure 22 shows that in the absence of FA, the overall performance of the process was better using nanotubes than nanoparticles. Additionally, at the same TiO_2 concentration, the nanoparticles removed 80% of the initial Hg(II) concentration, whereas the nanotubes resulted in almost complete removal. This can be due to the enhanced surface area and adsorption capabilities that the nanotubes offer as compared to the nanoparticles.

The addition of FA to the system enhanced the performance as explained in Section 4.3.2.4. However, when comparing the two different types of TiO_2, FA had a

higher effect with the nanoparticles than it did with the nanotubes, however >95% removals were achieved in both cases.

4.3.3 Kinetic Modelling of Hg(II) Removal

There is ongoing debate regarding the kinetics of photocatalytic degradation of aqueous pollutants by titanium dioxide. While numerous published articles hypothesize that the Langmuir-Hinshelwood (L-H) model best illustrates the kinetics [100], others claim that it is merely an easier way of interpreting data [101].

The L-H kinetic model relates the rate of degradation and concentration of target compounds in water as follows:

$$r = -\frac{dc}{dt} = \frac{k_r K_{ad} C}{1 + K_{ad} C} \quad (14)$$

Where r is the reaction rate, k_r is the L-H rate constant, K_{ad} is the adsorption equilibrium constant, C is the concentration of the target compound and t is the reaction time [102].

To interpret the results of this present study, it was first assumed that the data follow L-H kinetics. Rearrangement of Equation 14 results in the following:

$$\frac{1}{r} = \frac{1}{k_r K_{ad} C} + \frac{1}{k_r} \quad (15)$$

To validate this assumption, a plot of $\frac{1}{r}$ versus $\frac{1}{C}$ should yield a straight line with a slope of $\frac{1}{k_r K_{ad}}$ and an intercept of $\frac{1}{k_r}$. Results for $\frac{dC}{dt}$ were obtained by manually drawing tangents to the kinetic curves from Section 4.3.2 for each data point from initial to equilibrium conditions. The negative inverse of each $\frac{dC}{dt}$ data point resulted in $\frac{1}{r}$ values.

Plotting $\frac{1}{r}$ versus $\frac{1}{C}$ graphs for each condition lead to unrealistic results; while some graphs were not straight, those that were resulted in negative k_r and K_{ad} values. This shows that the data were not properly represented by the L-H model.

In the literature, little work is performed to model L-H kinetics, especially when using mercury as a contaminant. Most of the published models tend to approximate L-H kinetics as pseudo, or apparent, first order reaction [100] to simplify the model into a linear one (Equation 16).

$$r = -\frac{dC}{dt} = -k_{app}C \quad (16)$$

$$ln\frac{C}{C_0} = -k_{app}t \quad (17)$$

Where k_{app} is the apparent rate constant and C_0 is the initial contaminant concentration.

When investigating the validity of the pseudo first order model for the kinetic results of this study, it was observed that the plots of $ln\frac{C}{C_0}$ versus time yielded straight lines for the initial period of the testing (the first 10-15 minutes), after which it began to plateau despite the concentration decrease throughout the subsequent 15 minutes. Similar trends were observed in research performed by Ibhadon et al., where photocatalytic data fit the L-H model at initial stages of the reaction, after which degradation rates slowed down due to light scattering and adsorption effects [103].

Based on the above, L-H and the pseudo first order model were not able to explain the results of this present study. Ti-NT photocatalysis is associated with complex kinetics that is most likely due to the significant amount of Hg adsorption occurring on

the nanotubes alongside the degradation. This makes it challenging to develop a precise and accurate model to predict the removal of Hg removal by Ti-NT.

4.3.4 Evaluating Photocatalytic Reduction using XPS Results

Based on the results reported in Section 4.3.1, there is minimal Hg(II) adsorption occurring using TiO_2 nanoparticles, meaning that almost all the mercury removed was primarily due to photocatalytic reduction. However, unlike the nanoparticles, significant Hg(II) adsorption was shown using the Ti-NT. Although evidence of photoreduction was displayed by the higher Hg(II) removal in the presence of light, and by the results of continuous removal experiments summarized in Figures 20 and 21, further testing was conducted using XPS to determine the mercury speciation on the Ti-NT after treatment in order to determine if Hg(II) was removed by photoreduction or via adsorption.

Experiments were conducted in the light and dark at 10 mg/L initial Hg(II) concentration, using 1 g/L Ti-NT and 2.5mM formic acid. In order to collect a sufficient amount of solids for XPS analysis, ten times more Hg(II) and Ti-NT were used compared to the previous kinetic experiments. However, the ratio of Ti-NT: Hg(II) was maintained at the same ratio as in previous experiments. The solids were collected and filtered using vacuum filtration and were left to dry for 24 hours using a vacuum desiccator

Figure 24 illustrates the Hg (4f) spectra detected on the Ti-NT surface after 3 hours of reaction in the dark and 3 hours of irradiation under simulated sunlight. For both experiments, two sharp peaks of Hg (4f) appeared, however an eminent shift towards lower binding energies was observed for the sample under light, indicating that

the mercury exhibited a lower oxidation state, further supporting the hypothesis that photoreduction took place under light [104].

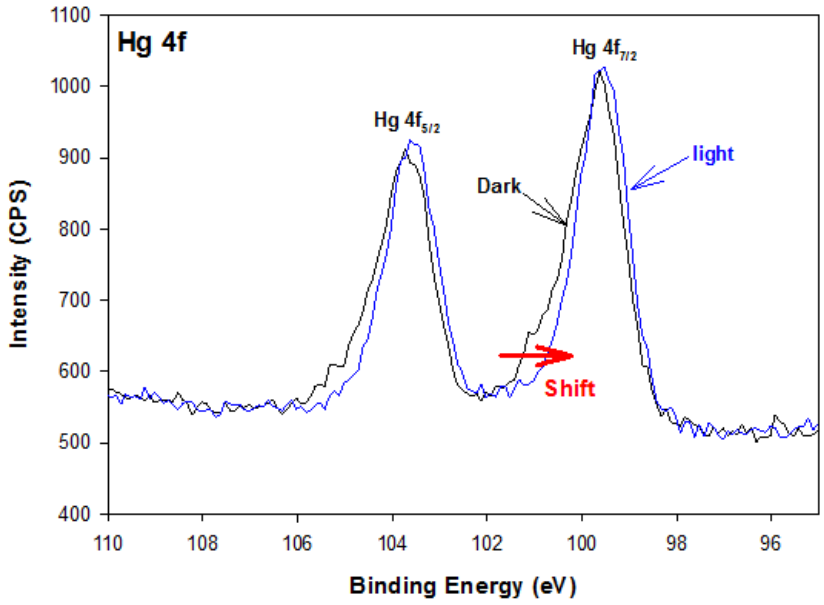

Figure 24: Hg (4f) spectra of the Ti-NT surface after 3 hours of Hg (II) adsorption in the dark and 3 hours of irradiation in the light

According to the NIST X-ray Photoelectron Spectroscopy Database, the major 4f $_{7/2}$ peaks of the most appropriate reference compounds for this study are: 99.7-99.9eV (Hg metal), 100.8 (Hg_2Cl_2) and 101.4 ($HgCl_2$). The major 4f $_{7/2}$ peaks of the XPS spectra shown in Figure 24 correspond mainly to elemental mercury. However, since there was a shift for the sample collected from experiment conducted under light, further analysis of the spectra deemed necessary.

XPS Peak 4.1 software was used to deconvolute the mercury peaks. Results summarized in Figures 25 and 26 indicate the presence of Hg(II), Hg (I) and Hg(0) on the Ti-NT solids in both dark and light conditions. However, the composition

percentages of these species varied as summarized in Table 21. According to these results, approximately equal amounts of Hg(II) were further reduced first into Hg (I) and subsequently into Hg(0). However, more reduction to the elemental mercury was observed under light than in the dark. Although there should be minimal Hg(II) reduction in the dark, the results obtained can be explained by the electron-hole generation as a result of X-ray irradiation within the XPS. Since the TiO_2 was bombarded with X-ray energy that is greater than the TiO_2's band gap energy, electron-hole pairs can form and reduction of Hg(II) into Hg(0) could occur. Electron-hole pair generation was also observed in the study conducted by Chenakin et. Al's as they evaluated the effect of XPS' X-rays on the surface chemical state of aluminum oxide, vanadium oxide and aluminovanadate oxide [105].

Since higher Hg(II) concentrations were expected to be present on the TiO_2 sample collected from experiments conducted in the dark than those collected from experiments conducted under light (before XPS analysis), more reduction could have occurred as a result of the XPS's X-ray irradiation in the former than the latter. Therefore, the higher percentage of elemental mercury on the sample experiments conducted under light is indicative of the occurrence of photoreduction.

While the XPS results support the occurrence of photoreduction, they are not very reliable in distinguishing the mercury speciation as a result of photoreduction verses adsorption. Consequently, an improvement of the method should be devised as a future step.

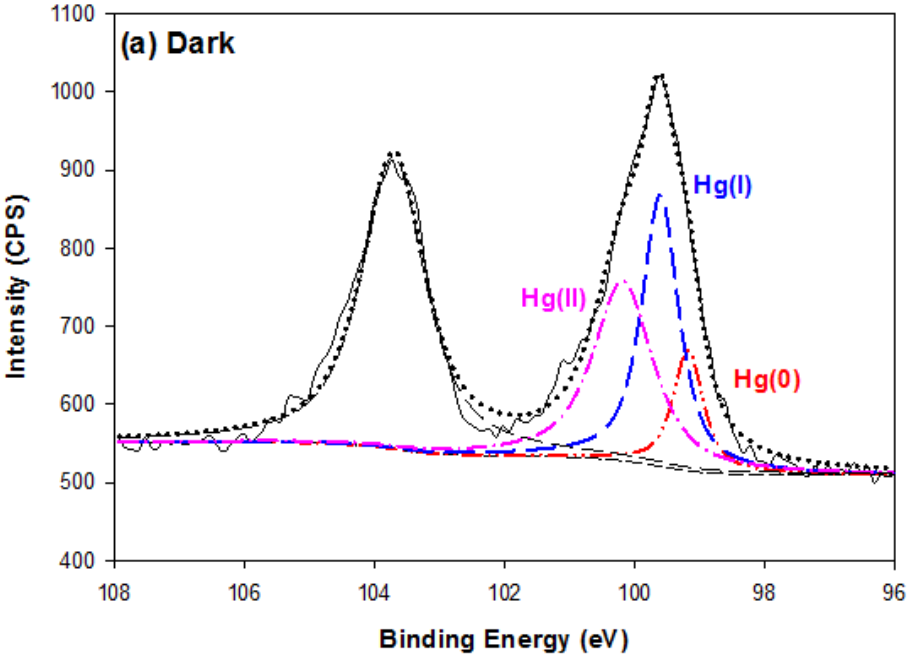

Figure 25: Hg (4f) spectra of Ti-NT surface after 3 hours of Hg(II) adsorption in the dark with peak deconvolution

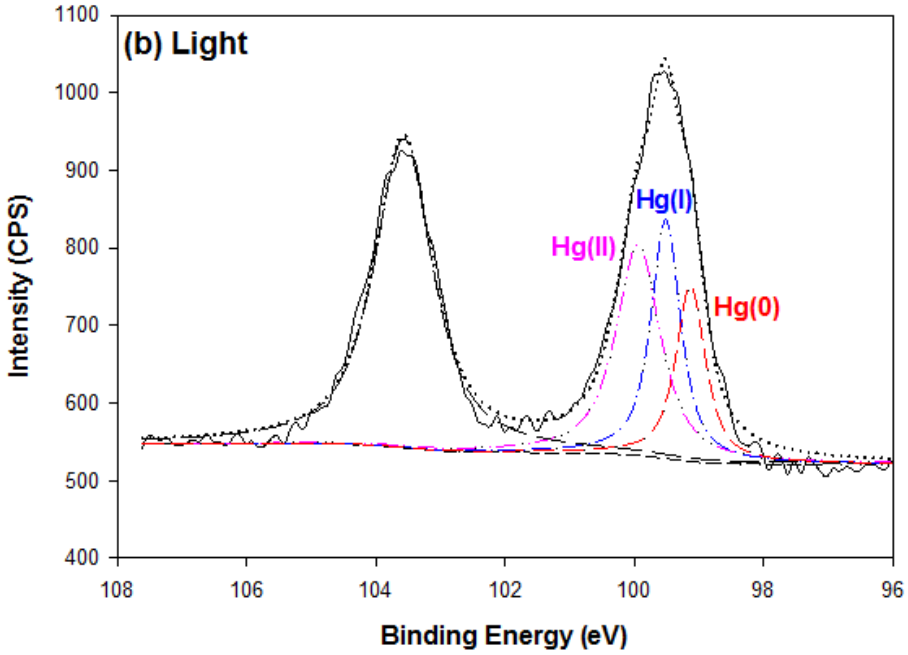

Figure 26: Hg (4f) spectra of Ti-NT surface after 3 hours of irradiation with peak deconvolution

Table 18: Composition percentage of Hg (4f) XPS spectra on Ti-NT sample

	Hg(0) %	Hg(I) %	Hg(II) %
Dark	14.9 %	41.2 %	43.7 %
Light	24.1 %	32.6 %	43.2 %

5. CONCLUSIONS

Mercury, especially in its aqueous form, is one of the most harmful contaminants present in water discharges due to its toxic and bio-accumulative properties. Photocatalysis is a process that utilizes a semiconductor photocatalyst and solar energy to remove contaminants, such as mercury, from water. For the photocatalytic degradation of mercury, a photocatalyst is employed to reduce aqueous mercury salts into its less toxic elemental form. Titanium dioxide is one of the most widely used photocatalysts due to its non-toxicity, high photocatalytic activity, enhanced chemical and thermal stability and its cost-effectiveness.

In this study, the removal of mercury using TiO_2 photocatalyst was characterized as affected by the following operating conditions: type and dosage of TiO_2, solution pH, irradiation time, and concentration of formic acid as a hole scavenger. Titanium dioxide nanotubes were synthesized in the lab via a hydrothermal process using a highly alkaline sodium hydroxide solution and microwave irradiation. The microwave digestion reaction took place in an hour at 1,600W.

TEM and SEM results revealed successful formation of nanotubes with a mean length and diameter of approximately 350 nm and 10 nm respectively. Additionally, XRD surface analysis of both nanoparticles and nanotubes indicated that the hydrothermal treatment did not affect the form of the TiO_2 precursor. However the nanotubes had broader and less intense peaks with an additional titanate peak forming at a 2θ value of 10^o due to microwave irradiation.

Experiments of mercury (II) removal from aqueous solutions were performed in the dark and under simulated sunlight irradiation to distinguish between physical adsorption and chemical reduction. In the presence of TiO_2 nanoparticles, negligible amount of Hg(II) removal was observed in the dark as compared to the light, indicating that photoreduction is indeed taking place.

Unlike the nanoparticles, TiO_2 nanotubes showed significant Hg(II) adsorption in the dark due to the larger surface area and more negative surface charge associated with the nanotubes. It was also observed that the Hg(II) adsorption strongly depended on the solution pH; with more removal at higher pH levels. This was explained by the surface chemistry of titanium dioxide as a function of pH; the surface charge of TiO_2 was more negative with increasing pH, causing less electrostatic repulsion to occur between the negatively charged catalyst and positively charged mercury. Similar trends were found under simulated light, where more photoreduction took place at higher pH levels. In addition to more adsorption taking place, higher pH levels result in a larger electron-driving-force (potential) in the titanium dioxide's conduction band and higher redox potentials of the mercury species.

When comparing the photocatalytic efficiency of nanoparticles and nanotubes, results showed that under simulated light, ten times more titanium dioxide nanoparticles than nanotubes were required to photoreduce the same amount of Hg(II). Additionally, for both types of TiO_2, photoreduction rate and efficiency increased at higher catalyst dosage and almost complete removal was observed when formic acid was added.

In summary, this study showed that the solar-driven photocatalytic treatment system using titanium dioxide photocatalyst is a green, sustainable, and cost-effective process for treating water with environmental contaminants such as mercury.

6. FUTURE RESEARCH

Future work can be conducted to better characterize the Hg(II) removal mechanism using TiO_2 nanotubes and model its kinetics. Additionally, the feasibility and effectiveness of reusing and recycling the TiO_2 nanotubes back into the system could be also investigated. This would enhance the cost-efficiency of the process and reduce the by-product waste associated with this technology. Other proposed future work is to evaluate the effect of oxygen and other types of hole scavengers on the performance of the photocatalytic system. Finally, because cost is a significant factor in research, the development of cost estimates for this technology would be another important future task to consider.

REFERENCES

[1] W. Xiao-jun, Z. Jian-yun, S. Shahid, X. Xing-hui, H. Rui-min, S. Man-ting, Catastrophe theory to assess water security and adaptation strategy in the context of environmental change, Mitigation Adapt. Strat. Global Change. 19 (2014) 463-477.

[2] C. Lipchin, E. Pallant, D. Saranga, A. Amster (Eds.), Integrated Water resources management and security in the Middle East, 1 ed., Springer, Netherlands, 2007.

[3] Qatar National Development Strategy 2011-2016, 1 ed., Gulf Publishing and Printing Company, Doha, Qatar, 2011.

[4] B. Dou, H. Chen, Removal of toxic mercury(II) from aquatic solutions by synthesized TiO2 nanoparticles, Desalination. 269 (2011) 260-265.

[5] J.M. Parks, A. Johs, M. Podar, R. Bridou, R.A. Hurt, S.D. Smith, S.J. Tomanicek, Y. Qian, S.D. Brown, C.C. Brandt, A.V. Palumbo, J.C. Smith, J.D. Wall, D.A. Elias, L. Liang, The genetic basis for bacterial mercury methylation, Science. 339 (2013) 1332-1335.

[6] L.B. Khalil, M.W. Rophael, W.E. Mourad, The removal of the toxic Hg(II) salts from water by photocatalysis, Applied Catalysis B: Environmental. 36 (2002) 125-130.

[7] K. Nakata, A. Fujishima, TiO 2 photocatalysis: design and applications, Journal of Photochemistry and Photobiology C: Photochemistry Reviews. 13 (2012) 169-189.

[8] A. Florea, D. Busselberg, Occurrence, use and potential toxic effects of metals and metal compounds, Biometals. 19 (2006) 419-427.

[9] I. Ji, The bioavailability of mercury in aquatic systems (2011).

[10] M.J. Lopez-Munoz, J. Aquado, A. Arencibia, R. Pascual, Mercury removal from aqueous solutions of $HgCl_2$ by heterogeneous photocatalysis with TiO_2, Applied Catalysis B: Environmental (2011).

[11] P. Floyd, P. Zarogiannis, M. Crane, S. Tarkowski, V. Bencko, Risks to health and the environment related to the use of mercury products (2002).

[12] E. Gonzaga, photocatalytic reduction of trace aqueous mercury using a visible light source (2014).

[13] US EPA Laws and Regulations.

[14] International Joint Commission, 12th biennial report on Great Lakes water quality (2004).

[15] D. Cappiello, New EPA rules aim to rein in toxic pollution, The Boston Globe (2011).

[16] US Enviromental Protection Agency, Treatment technologies for mercury in soil, waste, and water (2007).

[17] Norway to ban mercury, EU Business (2007).

[18] R.F. Edlich, S.L. Rhoads, H.S. Cantrell, S.M. Azavedo, A.T. Newkirk, Banning mercury amalgam, US FDA.

[19] Sweden to Ban Mercury, The Local (2009).

[20] H. Jones, EU bans mercury in barometers, thermometers, Reuters (2007).

[21] Governments at UN forum agree on legally-binding treaty to curb mercury pollution, UN News Centre (2013).

[22] J. De Clercq, Removal of mercury from aqueous solutions by adsorption on a new ultra stable mesoporous adsorbent and on a commercial ion exchange resin, International Journal of Industrial Chemistry (2012).

[23] D.L. Gallup, Removal of mercury from water in the petroleum industry.

[24] Executive by-law for the Environment Protection Law, Issued vide the Decree Law No. 30 for the Year 2002, The executive by-law (2002).

[25] J. Patterson, Aqueous mercury treatment, EPA. Capsule Report (1997).

[26] J.W. Patterson, Industrial wastewater treatment technology, 2 ed., Butterworth-Heinemann, 1985.

[27] J. Ritter, J. Bibler, Removal of mercury from waste water: Large-scale performance of an ion exchange process, Water Science & Technology. 25 (1992) 165-172.

[28] J.M. Grau, J.M. Bisang, Removal and recovery of mercury from chloride solutions by contact deposition on iron felt, Journal of Chemical Technology and Biotechnology. 62 (1995) 153-158.

[29] I. Wagner-Döbler, H. Von Canstein, Y. Li, K.N. Timmis, W. Deckwer, Removal of mercury from chemical wastewater by microoganisms in technical scale, Environ. Sci. Technol. 34 (2000) 4628-4634.

[30] X. Wang, S. Pehkonen, A.K. Ray, Photocatalytic reduction of Hg (II) on two commercial TiO_2 catalysts, Electrochim. Acta. 49 (2004) 1435-1444.

[31] I. Desai, , Mercury removal from aqueous systems using commercial and laboratory prepared metal oxide nanoparticles (2009).

[32] F. Di Natale, A. Erto, A. Lancia, D. Musmarra, Mercury adsorption on granular activated carbon in aqueous solutions containing nitrates and chlorides, J. Hazard. Mater. 192 (2011) 1842-1850.

[33] J.P. Gould, M.Y. Masingale, M. Miller, Recovery of silver and mercury from COD samples by ion cementation, Water Pollution Control Federation (1984) 280.

[34] B.B. Looney, M.E. Denham Jr, K.M. Vangelas, N.S. Bloom, Removal of mercury from low-concentration aqueous streams using chemical reduction and air stripping, J. Environ. Eng. 129 (2003) 819-825.

[35] Y. Uludag, H.Ö Özbelge, L. Yilmaz, Removal of mercury from aqueous solutions via polymer-enhanced ultrafiltration, J. Membr. Sci. 129 (1997) 93-99.

[36] F. Fu, Q. Wang, Removal of heavy metal ions from wastewaters: a review, J. Environ. Manage. 92 (2011) 407-418.

[37] W. Zhang, G. Huang, J. Wei, H. Li, R. Zheng, Y. Zhou, Removal of phenol from synthetic waste water using Gemini micellar-enhanced ultrafiltration (GMEUF), J. Hazard. Mater. 235 (2012) 128-137.

[38] M.A. Alka, M.K. Arvind, K. Shrirang, Removal of mercury from wastewater using micellar enhanced ultrafiltration, Res. J. Chem. Environ. 15 (2011) 624-628.

[39] K. Baek, J. Yang, T. Kwon, J. Yang, Cationic starch-enhanced ultrafiltration for Cr (VI) removal, Desalination. 206 (2007) 245-250.

[40] G.P. Broom, R.C. Squires, M.P.J. Simpson, I. Martin, The treatment of heavy metal effluents by crossflow microfiltration, J. Membr. Sci. 87 (1994) 219-230.

[41] Y. Terashima, H. Ozaki, M. Sekine, Removal of dissolved heavy metals by chemical coagulation, magnetic seeding and high gradient magnetic filtration, Water Res. 20 (1986) 537-545.

[42] N. Fowler, The pros and cons of filters, Canadian Industrial Machinery (2012).

[43] M. Mullett, L. Mohamed, Removal of mercury from solution using reverse osmosis filtration, Engineering our future: are we up to the challenge? 27-30 September 2009, Burswood Entertainment Complex (2009) 2207.

[44] K. Chakrabarty, P. Saha, A.K. Ghoshal, Separation of mercury from its aqueous solution through supported liquid membrane using environmentally benign diluent, J. Membr. Sci. 350 (2010) 395-401.

[45] I. Robles, T. Serrano, J. Pérez, G. Hernández, S. Solís, R. García, T. Pi, E. Bustos, Influence of EDTA on the electrochemical removal of mercury (ii) in soil from San Joaquín, Querétaro, México, Journal of the Mexican Chemical Society. 58 (2014) 332-338.

[46] H. Niroumand, R. Nazir, K.A. Kassim, The performance of electrochemical remediation technologies in soil mechanics, Int.J.Electrochem.Sci. 7 (2012) 5708-5715.

[47] H. Von Canstein, Y. Li, K.N. Timmis, Deckwer W., I. Wagner-Döbler, Removal of Mercury from Chloralkali Electrolysis Wastewater by a Mercury-Resistant*Pseudomonas putida* Strain, Applied and Environmental Microbiology. 65 (1995) 5729.

[48] C. Green-Ruiz, Mercury (II) removal from aqueous solutions by nonviable Bacillus sp. from a tropical estuary, Bioresour. Technol. 97 (2006) 1907-1911.

[49] M. Ebadian, M. Allen, Y. Cai, J.F. McGahan, Mercury contaminated material decontamination methods: investigation and assessment, Hemispheric Center for Environmental Technology, Florida International University, Miami, Final Report prepared for US Department of Energy, Office of Environmental Management, Office of Science and Technology. (2001).

[50] M.T. Amin, A.A. Alazba, U. Manzoor, A review of removal of pollutants from water/wastewater using different types of nanomaterials, Advances in Materials Science and Engineering. 2014 (2014) 24.

[51] P.N. Dave, L.V. Chopda, Application of iron oxide nanomaterials for the removal of heavy metals, Journal of Nanotechnology. 2014 (2014).

[52] P.Z. Ray, H.J. Shipley, Inorganic nano-adsorbents for the removal of heavy metals and arsenic: a review, RSC Advances. 5 (2015) 29885-29907.

[53] S. Pacheco, M. Medina, F. Valencia, J. Tapia, Removal of inorganic mercury from polluted water using structured nanoparticles, J. Environ. Eng. 132 (2006) 342-349.

[54] J. Pandipriya, E. Praveena, R.M. Kuriakose, Suganiya, J.A. Marcilin, M. Therese, N.M. Nandhitha, An insight into the selection of nano particle for removing contaminants in waste water, International Journal of Engineering Research and Applications. 4 (2014).

[55] K. Lisha, S.M. Maliyekkal, T. Pradeep, Manganese dioxide nanowhiskers: a potential adsorbent for the removal of Hg (II) from water, Chem. Eng. J. 160 (2010) 432-439.

[56] D. Pei, J. Luan, Development of visible light-responsive sensitized photocatalysts, International Journal of Photoenergy. 2012 (2011).

[57] M.A. Quiroz, C.A. Martínez-Huitle, E.R. Bandala, Advanced oxidation processes (AOPs) for removal of pesticides from aqueous media, INTECH Open Access Publisher, 2011.

[58] A.L. Linsebigler, G. Lu, J.T. Yates Jr, Photocatalysis on TiO2 surfaces: principles, mechanisms, and selected results, Chem. Rev. 95 (1995) 735-758.

[59] J.M. Herrmann, Heterogeneous photocatalysis: state of the art and present applications, Topics in Catalysis. 34 (2005) 49.

[60] H. Hennig, R. Billing, Advantages and disadvantages of photocatalysis induced by light-sensitive coordination compounds, Coord. Chem. Rev. 125 (1993) 89-100.

[61] H. De Lasa, B. Serrano-Rosales, Advances in chemical engineering: photocatalytic technologies, Academic Press, 2009.

[62] J. Xu, X. Xiao, F. Ren, W. Wu, Z. Dai, G. Cai, S. Zhang, J. Zhou, F. Mei, C. Jiang, Enhanced photocatalysis by coupling of anatase TiO2 film to triangular Ag nanoparticle island, Nanoscale research letters. 7 (2012) 1-6.

[63] Y. Zeng, Y. Liu, Y. Lu, J. Chung, Study on the preparation of nanosized titanium dioxide with tubular structure by hydrothermal method and their photocatalytic activity.

[64] L.L. Costa, A.G. Prado, TiO_2 nanotubes as recyclable catalyst for efficient photocatalytic degradation of indigo carmine dye, J. Photochem. Photobiol. A. 201 (2009) 45-49.

[65] M. Zlamal, J.M. Macak, P. Schmuki, J. Krýsa, Electrochemically assisted photocatalysis on self-organized TiO2 nanotubes, Electrochemistry Communications. 9 (2007) 2822-2826.

[66] M. Castellote, N. Bengtsson, Principles of TiO_2 photocatalysis, in: applications of titanium dioxide photocatalysis to construction materials, Springer, 2011, pp. 5-10.

[67] J. Zhang, P. Zhou, J. Liu, J. Yu, New understanding of the difference of photocatalytic activity among anatase, rutile and brookite TiO_2, Phys.Chem.Chem.Phys. 16 (2014) 20382-20386.

[68] T. Luttrell, S. Halpegamage, J. Tao, A. Kramer, E. Sutter, M. Batzill, Why is anatase a better photocatalyst than rutile?-Model studies on epitaxial TiO_2 films, Scientific reports. 4 (2014).

[69] G. Li, C.P. Richter, R.L. Milot, L. Cai, C.A. Schmuttenmaer, R.H. Crabtree, G.W. Brudvig, V.S. Batista, Synergistic effect between anatase and rutile TiO_2 nanoparticles in dye-sensitized solar cells, Dalton Transactions (2009) 10078-10085.

[70] T. Ohno, K. Sarukawa, K. Tokieda, M. Matsumura, Morphology of a TiO_2 photocatalyst (Degussa, P-25) consisting of anatase and rutile crystalline phases, Journal of Catalysis. 203 (2001) 82-86.

[71] I. Tacchini, A. Ansón-Casaos, Y. Yu, M.T. Martinez, M. Lira-Cantú, Hydrothermal synthesis of 1D TiO_2 nanostructures for dye sensitized solar cells, Materials Science and Engineering: B. 177 (2012) 19-26.

[72] X. Wu, Q. Jiang, Z. Ma, M. Fu, W. Shangguan, Synthesis of titania nanotubes by microwave irradiation, Solid State Commun. 136 (2005) 513-517.

[73] T. Kasuga, M. Hiramatsu, A. Hoson, T. Sekino, K. Niihara, Formation of titanium oxide nanotube, Langmuir. 14 (1998) 3160-3163.

[74] A. Pucci, K.R. Wandelt, Physics and engineering of new materials, Springer Science & Business Media, 2009.

[75] C. Huang, Y. Yang, R. Doong, Microwave-assisted hydrothermal synthesis of mesoporous anatase TiO 2 via sol–gel process for dye-sensitized solar cells, Microporous and Mesoporous Materials. 142 (2011) 473-480.

[76] N. Moloto, S. Mpelane, L.M. Sikhwivhilu, S. Sinha Ray, Optical and morphological properties of ZnO-and TiO_2-derived nanostructures synthesized via a microwave-assisted hydrothermal method, International Journal of Photoenergy. 2012 (2012).

[77] T. Tan, D. Beydoun, R. Amal, Effects of organic hole scavengers on the photocatalytic reduction of selenium anions, J. Photochem. Photobiol. A. 159 (2003) 273-280.

[78] Z. Peng, H. Tang, Y. Tang, K.F. Yao, H.H. Shao, Synthesis and photocatalytic activity of magnetically recoverable core-shell nanoparticles, International Journal of Photoenergy. 2014 (2014).

[79] R. GH, A. Firuzian., H. P, Microwave-assisted synthesis of TiO_2 nanotube: influence of irradiation power, temperature and pressure on its photocatalytic activity and morphology, Proceedings of the 4th International Conference on Nanostructures (ICNS4) (2012).

[80] E. Kopysc, K. Pyrzynska, S. Garbos, E. Bulska, Determination of mercury by cold-vapor atomic absorption spectrometry with preconcentration on a gold-trap, Analytical sciences. 16 (2000) 1309-1312.

[81] P.S. - Mann, - Introductory Statistics.

[82] L.M. Sikhwivhilu, S. Mpelane, N. Moloto, S. Sinha Ray, Hydrothermal synthesis of TiO_2 nanotubes: microwave heating versus conventional heating (2010).

[83] Kustiningsih, I., ., S., Purwanto,W., Synthesis of titania nanotubes and titania nanowires by combination sonication-hydrothermal treatment and their photocatalytic activity for hydrogen production, International Journal of Technology. 5 (2014).

[84] J.A. Knoll, N. Pennisi, P.A. Yarnell, Synthesis of sodium titanate and ion exchange use thereof (2013).

[85] D.L. Morgan, Alkaline hydrothermal treatment of titanate nanostructures (2010).

[86] A.V. Naumkin, A. Kraut-Vass, S.W. Gaarenstroom, C.J. Powell, NIST X-ray Photoelectron Spectroscopy Database (September 15, 2012).

[87] S.G. Botta, D.J. Rodríguez, A.G. Leyva, M.I. Litter, Features of the transformation of HgII by heterogeneous photocatalysis over TiO_2, Catalysis Today. 76 (2002) 247-258.

[88] N. Serpone, Y. Ah-You, T. Tran, R. Harris, E. Pelizzetti, H. Hidaka, AM1 simulated sunlight photoreduction and elimination of Hg (II) and CH3Hg (II) chloride salts from aqueous suspensions of titanium dioxide, Solar Energy. 39 (1987) 491-498.

[89] D. Chen, A. K. Ray, Removal of toxic metal ions from wastewater by semiconductor photocatalysis, Chemical Engineering Science. 56 (2001) 1561-1570.

[90] H. Liang, X. Li, J. Nowotny, Photocatalytic properties of TiO_2 nanotubes.

[91] W. Liu, J. Gao, F. F Zhang, G. Zhang, Preparation of TiO2 nanotubes and their photocatalytic properties in degradation methylcyclohexane, Materials Transactions. 48 (2007) 2464-2466.

[92] K.M. Krupka, D. Kaplan, G. Whelan, R. Serne, S. Mattigod, Understanding variation in partition coefficient, Kd, values, Volume II: Review of Geochemistry and Available K_d Values, for Cadmium, Cesium, Chromium, Lead, Plutonium, Radon, Strontium, Thorium, Tritium (3H), and Uranium.EPA (1999).

[93] K.E. Engates, H.J. Shipley, Adsorption of Pb, Cd, Cu, Zn, and Ni to titanium dioxide nanoparticles: effect of particle size, solid concentration, and exhaustion, Environmental Science and Pollution Research. 18 (2011) 386-395.

[94] W. Yantasee, C.L. Warner, T. Sangvanich, R.S. Addleman, T.G. Carter, R.J. Wiacek, G.E. Fryxell, C. Timchalk, M.G. Warner, Removal of heavy metals from aqueous systems with thiol functionalized superparamagnetic nanoparticles, Environ. Sci. Technol. 41 (2007) 5114-5119.

[95] A. Assadi, M.H. Dehghani, N. Rastkari, S. Nasseri, A.H. Mahvi, Photocatalytic reduction of hexavalent chromium in aqueous solutions with zinc oxide nanoparticles and hydrogen peroxide, Environ. Prot. Eng. 38 (2012) 5-16.

[96] P. Mitra, P. Banerjee, S. Chakrabarti, S. Bhattacharjee, Utilization of solar energy for photoreduction of industrial wastewater containing hexavalent chromium with zinc oxide semiconductor catalyst, Desalination and Water Treatment. 51 (2013) 5451-5459.

[97] A.H. Ali, Study on the photocatalytic degradation of indigo carmine dye by TiO_2 photocatalyst, Journal of Kerbala University. 11 (2013).

[98] N. Liu, X. Chen, J. Zhang, J.W. Schwank, A review on TiO_2-based nanotubes synthesized via hydrothermal method: Formation mechanism, structure modification, and photocatalytic applications, Catalysis Today. 225 (2014) 34-51.

[99] G. Lenzi, C. Fávero, L. Colpini, H. Bernabe, M. Baesso, S. Specchia, O. Santos, Photocatalytic reduction of Hg (II) on TiO 2 and Ag/TiO 2 prepared by the sol–gel and impregnation methods, Desalination. 270 (2011) 241-247.

[100] A. Idris, N. Hassan, R. Rashid, A. Ngomsik, Kinetic and regeneration studies of photocatalytic magnetic separable beads for chromium (VI) reduction under sunlight, J. Hazard. Mater. 186 (2011) 629-635.

[101] A. Emeline, V. Ryabchuk, N. Serpone, Dogmas and misconceptions in heterogeneous photocatalysis. Some enlightened reflections, The Journal of Physical Chemistry B. 109 (2005) 18515-18521.

[102] S. Y, Effective Photocatalytic Reduction of Cr(VI) by carbon modified (CM)-n-TiO2 nanoparticles under solar irradiation, World Journal of Nano Science and Engineering. Vol. 3 No. 4 (2013) 154.

[103] A. Ibhadon, Investigating the kinetics and mechanisms of the photocatalytic degradation of Azo compounds by irradiated semiconductor materials, Trends in Photochemistry & Photobiology. 16 (2014) 27.

[104] F.C. Krebs, Polymer photovoltaics: A Practical Approach, Society of Photo Optical, 2008.

[105] S. Chenakin, R. Prada Silvy, N. Kruse, Effect of X-rays on the surface chemical state of Al2O3, V2O5, and aluminovanadate oxide, The Journal of Physical Chemistry B. 109 (2005) 14611-14618.